SIZE MODULATION AND DEFECTS IN GRAPHENE BASED RIBBONS: MAGNETISM AND CHARGE CONFINEMENT

A THESIS

SUBMITTED TO THE PROGRAM OF MATERIAL SCIENCE AND

NANOTECHNOLOGY

AND THE INSTITUTE OF ENGINEERING AND SCIENCE

OF BILKENT UNIVERSITY

IN PARTIAL FULFILLMENT OF THE REQUIREMENTS

FOR THE DEGREE OF

MASTER OF SCIENCE

By

Mehmet Topsakal

July, 2008

I certify that I have read this thesis and that in my opinion it is fully adequate, in scope and in quality, as a thesis for the degree of Master of Science.

Prof. Dr. Salim Çıracı (Advisor)

I certify that I have read this thesis and that in my opinion it is fully adequate, in scope and in quality, as a thesis for the degree of Master of Science.

Assist. Prof. Dr. Mehmet Bayındır

I certify that I have read this thesis and that in my opinion it is fully adequate, in scope and in quality, as a thesis for the degree of Master of Science.

Assoc. Prof. Dr. Ulrike Salzner

Approved for the Institute of Engineering and Science:

Prof. Dr. Mehmet B. Baray
Director of the Institute Engineering and Science

ABSTRACT

SIZE MODULATION AND DEFECTS IN GRAPHENE BASED RIBBONS: MAGNETISM AND CHARGE CONFINEMENT

Mehmet Topsakal
M.S. in Material Science and Nanotechnology
Supervisor: Prof. Dr. Salim Çıracı
July, 2008

In this thesis, we investigated the effects of vacancy and heterojunction formation on electronic and magnetic properties of graphene nanoribbons (GNRs) by using first principles pseudopotential plane wave method within Density Functional Theory. Graphene based materials are expected to be very important in future technology. Through understanding of all the factors which influence their physical properties is essential. We have shown that electronic and magnetic properties of graphene nanoribbons can be affected by defect-induced itinerant states. The band gaps of armchair nanoribbons can be modified by hydrogen saturated holes. Defects due to periodically repeating vacancies or divacancies induce metallization, as well as magnetization in non-magnetic semiconducting nanoribbons due to the spin-polarization of local defect states. Antiferromagnetic ground state of semiconducting zigzag ribbons can change to ferrimagnetic state upon creation of vacancy defects, which reconstruct and interact with edge states. Even more remarkable is that all these effects of vacancy defects are found to depend on their geometry and position relative to edges. We also predicted that periodically repeated junctions of graphene ribbons of different widths form multiple quantum well structures having confined states. These quantum structures are unique, since both constituents of heterostructures are of the same material. The width as well as the band gap, for specific superlattices are modulated in direct space. Orientation of constituent nanoribbons, their widths, lengths and the symmetry of the junction are some of the crucial structural parameters to engineer electronic properties of these systems. Our further studies on nanoribbons and nanoribbon superlattices showed the strong dependence of band gaps and magnetic moments on applied uniaxial stress. This thesis presents an extensive

study of size modulation and defect formation on graphene nanoribbons.

Keywords: ab initio, density functional theory, graphene, graphene nanoribbons, defects, elasticity, superlattices, confinement, multiple quantum well structures .

ÖZET

GRAFİN TABANLI MALZEMELERDE KALINLIKSAL ÇEŞİTLENDİRMELER VE AĞ ÖRGÜ DELİKLERİ: MANYETİZMA VE YÜK YOĞUNLAŞMASI

Mehmet Topsakal
Malzeme Bilimi ve Nanoteknoloji Enstitüsü , Yüksek Lisans
Tez Yöneticisi: Prof. Dr. Salim Çıracı
Temmuz, 2008

Bu tezde grafin nanoşeritlerin elektronik ve manyetik özelliklerinin ağ örgü deliklere ve heterojen kesit oluşumuna göre nasıl değiştiğini pseudo potansiyelli düzlem dalga metodlu yoğunluk fonksiyoneli teorisi ile inceledik. Grafin tabanlı malzemelerin geleceğin teknolojisinde oldukça önemli bir yere sahip olması beklenmektedir ve bu yüzden bu malzemenin fiziksel özelliklerini belirleyen faktölerin iyi anlaşılması gerekmektedir. Biz gösterdik ki grafin şeritlerin elektronik ve manyetik özellikleri delik sonucu oluşan dalga durumları yüzünden oldukça fazla etkilenmektedir. Armchair türü grafin şeritlerin yasak enerji aralıkları hidrojenle doyurulmuş delikler sayesinde modifiye edilebilmektedir. Bu delikler malzemeye metalik özellik kazandırabilmekte hatta manyetik olmayan armchair şeritlere yerel manyetik özellikler dahi kazandırabilmektedir. Zigzag türü grafin şeritlerde ise kenar durumlarının delik yüzünden oluşan durumlar ile etkileşmesi sonucu antiferromagnetik halden ferrimagnetic hale geçiş gözlemlenmektedir. Daha da ilginci bütün bu etkiler deliğin yapısına ve oluştuğu yere göre değişiklikler göstermektedir. Deliklerden ayrı olarak bizler farklı kalınlıktaki grafin şeritlerin birleştirilmesi ile oluşturulan grafin yapılarının çoklu kuantum kuyu yapılarının oluşturduklarını da gösterdik. Yeni yapıyı oluşturan bileşenler aynı malzeme olduğu için bu sistemler geleneksel heterojen yapılardan farklılık göstermektedir. Heterojen sistemi oluşturan şeritlerin kalınlıkları ve boyları, birbirlerine olan konumları, simetrileri heterojen sistemin elektronik özelliklerinin kontrol edilmesinde önemli rol oynamaktadır. Daha ileriki çalışmalarımız, grafin şeritleri ve onların farklı kalınlıklarının birleştirilmesi ile oluşturulan heterojen yapıların yasak enerji aralıklarının uygulanılan gerilme ile değiştiğini de göstermektedir. Bu tez yukarıda anlattığımız bütün etkenlerin grafin şeritlerine olan etkilerinin incelendiği kapsamlı bir çalışmayı sunmaktadır.

Anahtar sözcükler: temel prensipler, yoğunluk fonksiyoneli teorisi, grafin, grafin şeritler, ağ örgü boşlukları, elastik özellikler, süperörgüler, yük yoğunlaşmaları, çoklu kuantum kuyu yapıları .

Acknowledgement

I would like to express my deepest gratitude and respect to my supervisor Prof. Dr. Salim Çıracı for his patience and guidance during this research and also for giving me a chance to be one of his assistant.

I am thankful to Assoc. Prof. Dr. Mehmet Bayındır for his motivation and guidance for me and all MSN students.

I would like to thank to Dr. Haldun Sevinçli and Ethem Aktürk for being my research-partners.

I would like to thank to all other group members Erman Bekaroğlu, Seymur Cahangirov and Can Ataca.

I would like to also thank Hasan Şahin and his advisor Assist. Prof. Dr. R. Tuğrul Senger for their valuable discussions.

I would like to thank all my friends in Institute of Material Science and Nanotechnology and Physics Department for their friendship.

I bless my mother and father for their endless love and support.

Contents

List of Figures

Chapter 1

Introduction

Carbon is one of the most interesting elements in periodic table. It is found in many phases and allotropes [1] such as graphite and diamond which are known from ancient times and carbon nanotubes and fullerenes which have been discovered in near history. Graphene, the honeycomb structure of sp^2-hybridized carbon atoms, which is the building block of graphite, CNTs, C_{60} and some other forms of carbon, was presumed not to exist in free form while its allotropes have been the subject of intensive research in past two decades.

Graphene is a strictly two-dimensional (2D) material; its stability has been treated by Landau and Peierls [2, 3] . They concluded that any 2D crystals are unstable by showing that , in the standard harmonic approximation, thermal fluctuations should disturb the long-range order of the crystals and making them melted at any temperature [4]. Also Mermin and Wagner drew similar conclusions on the subject [5]. From the experimental point of view, thin films or similar structures have lost their stability after a certain thickness, i.e 10-15 atomic layers, segregating into islands or decomposing [6].

Unexpectedly, in 2004, scientists have managed to isolate 2D crystals of graphene at room temperature [8] which was thought to be impossible for a long time. Despite earlier theories against the exiastence of perfect 2D crystals, a detailed analysis of thel problem beyond the harmonic approximation has led to the

conclusion that the interaction between bending and stretching long-wavelenght phonons could in principle stabilize atomically thin membranes through their deformation in the third dimension [7]. Indeed, Andre Geim, Kostya Novoselov and co-workers produced two dimensional crystals of graphene by delicately cleaving a sample of graphite with a sticky tape, and was able to visualize the new crystal by using a simple optical microscope [8].

In the beginning, the graphene synthesis didn't attract interest. Further investigations on graphene revealed some unusual properties and graphene is now a subject of very intensive study. Following studies brought about several new concepts into the condensed matter physics, such as charge carriers resembling the Dirac spectrum for massles fermions [9], anomalous (integer and half integer) quantum hall effect [10], ballistic transport at room temperature [8], chiral tunnelling and the Klein paradox [11] ... some of which have been predicted theoretically and verified experimentally.

The electrons of graphene somehow behave differently than ordinary electrons. The special relativity tells us that the energy of a free particle is given by the equation E=$\sqrt{m^2c^4 + p^2c^2}$ where m and p are the mass and momentum of the particle respectively. For electrons corresponding to Bloch waves in a solid, the mass m is called the "band mass", and it is not necessarily equal to the mass of a free electron. This band mass effects most of the electronic properties of metals and semiconductors, such as their ability to carry electrical current. The interactions between electrons and the honeycomb lattice of carbon atoms in graphene causes the electrons to behave as if they have no mass. The energy relation turns into E=pv for graphene where v is the "Fermi-Dirac velocity". This linear relationship with momentum is just like the case for a photon. The only difference is the magnitude of v which is 1/300 of the speed of light. Interestingly, these novel properties provide a way to probe quantum electrodynamics (QED) phenomena without the need of huge particle accelerators by measuring graphene's electronic properties.

In addition to the Dirac-fermion like spectrum of electrons in graphene, there is another odd property that electrons can travel long distances without colliding

with any impurities, even at room temperatures [8]. Carbon atoms have four electrons available for bonding. By making 3 bonds in 2D hexagonal structure, one unbound electron is free to wander through the crystal, attributing graphene distinctive characteristics - excellent conductivity. In ordinary metals, electron scattering leads to energy loss and this limits the abilities of today's electronic devices. In contrast graphene seems to be an exceptional choice for tomorrow's electronics.

Carbon nanotubes and fullerenes have been studied extensively in the past two decades. Many interesting properties have been revealed and remarkable applications have been suggested. To a large extent, the electronic properties of carbon nanotubes have their origins from graphene. So that graphene studies can benefit from the relatively matured research on CNTs and fullerenes. A quick adaptation can lead to improvement of carbon based electronics to reach industrial stage. Unlike CNTs, graphene production seems to be relatively easy and with the advance of new techniques large amounts of graphene quantities can be produced.

1.1 Motivation

Graphene is an example of a truly two dimensional crystal with interesting properties. Carbon based materials are expected to be building block of tomorrow's technology. Carbon nanotubes can be metallic or semiconducting, depending on their chirality. This could lead to a fully carbon-based elecronics. However, the present lack of control on the chirality prevents carbon nanotubes from engineering their electronic properties; and this is a major barrier to industrial implementation. Recent studies indicate that graphene nanoribbons can be produced in a highly controlable manner unlike CNTs [12]. Graphene nanoribbons appear to be superior to nanotubes.

In spite of the fact that the first graphene samples have been obtained in 2004, some realistic applications have already been developed. A few interesting works

may give the reader the idea about the endless applications and help the reader to understand the high scientific interest on graphene.

The use of graphene based materials in nanoelectronics is one of the promising areas. A graphene ballistic transistor is an application which first comes to mind. Professor Andre Geim and Dr Kostya Novoselov from The School of Physics and Astronomy at The University of Manchester claim to have created transistors that are just one atom-thick and less than 50 atoms wide from a new class of material [8, 13]. Graphene exhibits a pronounced response to perpendicular external electric field allowing one to built FETs. Crucially, the transistor operates at room temperature making it potentially valuable for future electronic components. Such circuits include the central element, or "quantum dot", semitransparent barriers to control the movement of individual electrons, interconnects and logic gates - all made entirely of graphene. Since the silicon based technologies are approaching their fundamental limits, graphene may offer an exceptional choice.

The use of graphene powder in electric batteries is another promising application. A huge surface-to-volume ratio and high conductivity provided by graphene powder can lead to improve the efficiency of batteries, taking over from the carbon nanofibres used in modern batteries. Carbon nanotubes have also been considered for this application but graphene powder has an important advantage of being inexpensive to produce [14].

The use of graphene as sensor is also important. Again Gaim and colleagues, created micrometre-sized flakes of graphene by micromechanical cleavage of graphite at the surface of oxidized silicon wafers. The researchers then used electron beam lithography to make electrical contacts on the flake. A single flake, around 10 micrometres across, was placed in a chamber and its electrical resistance measured as dilute nitrogen dioxide was slowly leaked in. The researchers observed distinct and discrete step changes in resistance, corresponding to single molecules of the gas adsorbing to and desorbing from the graphene flake [15]..

Functionalization of graphene by adatoms can also provide endless applications. Chemical functionalization and substitutional doping have been investigated for many years in nanotubes with the aim of tailoring their properties for

sensing, transport, and chemical and optical applications. It is thus natural to do a similar investigation for graphene. Hydrogen storage is one of the very active research areas and it was theoretically predicted that lithium decorated graphene can absorb a large amount of hydrogen [16]. On the other hand, transition metal (TM) atom adsorption metallizes graphene and adds magnetic properties. It was predicted that Fe and Ti adsorption can make graphene nanoribbons half-metallic with 100 % spin polarization at Fermi level [17] providing a very important material for spintronic applications.

Graphene nanoribbons are very narrow structures of graphene and might have crucial importance in future nanotechnology applications. They might be building blocks of graphene transistor networks that we mentioned above, half metallic material for future spintronic devices [42]. The experimental synthesis of GNRs with well defined shapes was recently done by some researchers [12]. Magnetic edge states of graphene nanoribbons were predicted by some early theoretical works [44] . Also the strong dependence of band gaps of graphene nanoribbons with their widths was predicted by some first-principles calculations [41] and this was proved by a recent experimental work [21] . However, to our knowledge, first-principles calculations on the effects of vacancies and heterojunction formation of graphene nanoribbons have not been performed. We believe that such analyses are necessary for graphene nanoribbons. In this thesis we aim to explore the electronic and magnetic properties of graphene ribbons with the hope of some new device applications.

1.2 Organization of the Thesis

The thesis is organized as follows: Chapter 2 summarizes the basic properties of graphene and graphene nanoribbons, Chapter 3 is devoted to the theoretical background. In Chapter 4, our results are presented. Finally in Chapter 4, important conclusion of thesis is summarized.

Chapter 2

Graphene and Graphene Nanoribbons

Graphene, graphite, CNTs and fullerenes are categorized in carbon-based π electron systems in honeycomb network, which are distinguished from sp^3-based nanocarbon systems having a tetrahedral network such as diamond. With the sp^2 hybridization of one s-orbital and two p-orbitals results in a triangular planar structure with a formation of a σ-bond between carbon atoms which are seperated by 1.42 Å.

The perfect 2D graphene is an infinite network of hexagonal lattice, in contrast to ideal graphene which is a nanosized flat hexagon network with the presence of open edges around its periphery. The open edges become important for nanoribbons.

2.1 Structure of Graphene

The structure of graphene layers have been explored by using the high resolution microscopy techniques such as Raman [19] and Rayleigh [20]. The graphene structures based on the hexagonal lattice of carbon atoms have been confirmed [13].

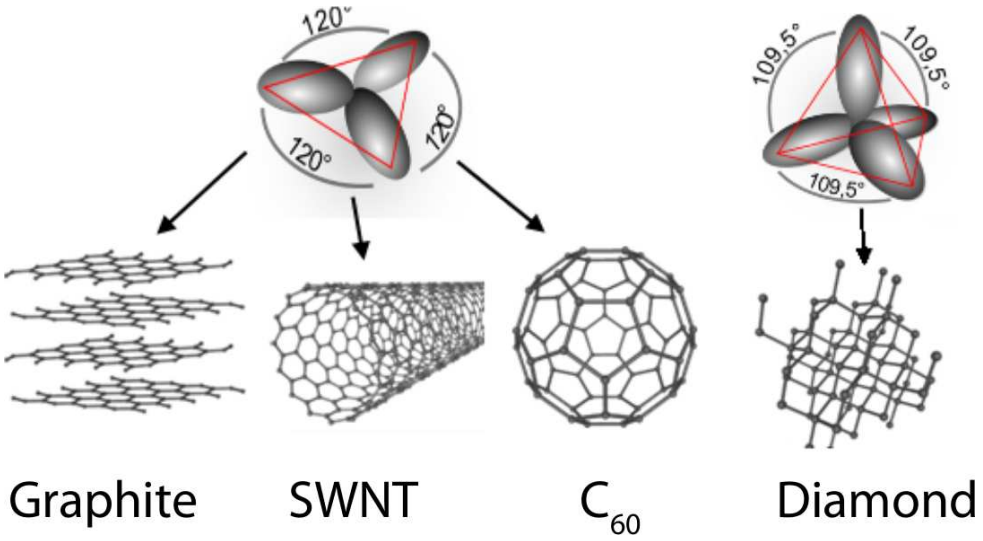

Figure 2.1: Graphene, graphite, single-walled carbon nanotube (SWNT) and C_{60} structures make sp^2 type bonding, whereas diamond makes sp^3 type bonding. Graphite can be viewed as a stack of graphene layers. Carbon nanotubes are rolled up cylinders of graphene and fullerenes are the molecules consisting of wrapped graphene by the introduction of pentagons on the hexagonal structure. The diamond is a transparent crystal of tetrahedrally bonded carbon atoms and crystallizes into the face centered cubic lattice structure.

Once identied, graphene layers can be processed into nanoribbons by lithography techniques [21].

One carbon atom in honeycomb structure bound to three neighbour through strong, covalent bonds. This configuration gives exceptional structural rigidity within its layers.

The structure is not a Bravais lattice but it can be seen as a triangular lattice with a basis of two atoms per unit cell. The lattice vectors can be written as :

$$a_1 = \frac{a}{2}(3, \sqrt{3}, 0) \qquad a_2 = \frac{a}{2}(3, -\sqrt{3}, 0) \tag{2.1}$$

where a $\approx$ 1.42 Å is the C-C distance. The reciprocal lattice vectors are given by :

$$b_1 = \frac{2\pi}{3a}(1, \sqrt{3}, 0) \qquad b_2 = \frac{2\pi}{3a}(3, -\sqrt{3}, 0) \tag{2.2}$$

The two points at the corners of graphene's Brillouin zone (BZ) is of special importance. They are named Dirac points. Their positions are given by:

$$K = \left(\frac{2\pi}{3a}, \frac{2\pi}{3\sqrt{3}a}, 0\right) \qquad K' = \left(\frac{2\pi}{3a}, -\frac{2\pi}{3\sqrt{3}a}, 0\right) \tag{2.3}$$

2.2 Synthesis

Graphene sheets (a single sheet or a few layer sheet) can mainly be prepared by micromechanical cleaving of graphite crystals according to recent experiments [8, 9, 10] or by epitaxial growth on silicon carbide (SiC) [22, 23]. The first method can be used to obtain high quality of graphene sheets which are comparable to

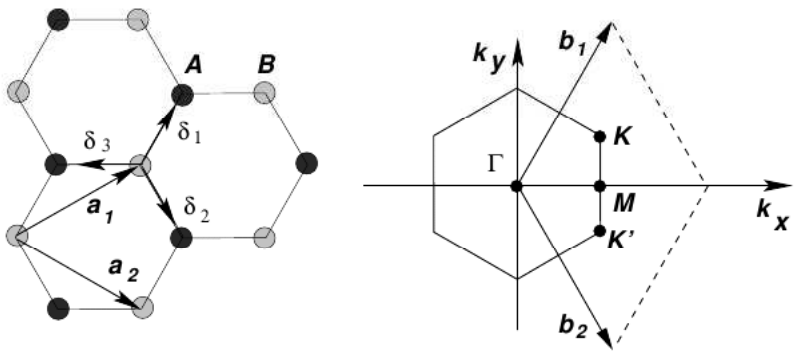

Figure 2.2: Left: Lattice structure of graphene made of two interpenetrating hexagonal lattices (a_1 and a_2 are lattice unit vectors, and δ_i , i=1,2,3 are the nearest neighbor vectors); Right: corresponding Brillouin zone. The Dirac corners sit at the K and K' points.

that in graphite, but it is restricted by small sample dimensions and low visibility. On the other hand, the second one is more suitable for large area fabrication and is more compatible with current Si processing techniques for future applications. Nevertheless, the epitaxial graphene was shown to interact with SiC by first principles calculations [24, 25] and experiments [26, 27].

2.3 Electronic Properties of Graphene

The investigations of electronic properties of graphene trace back to 1946 when P. R. Wallace wrote the first scientific paper on the band structure of graphene as an approximation trying to understand the electronic properties of more complex, three dimensional (3D) graphite. He did not use the word graphene and referred to "a single hexagonal layer " [18]. The electrical properties of graphene can be described by a conventional tight-binding model; in this model the energy of the electrons with wavenumber **k** is

$$E = \pm\sqrt{\gamma_0^2\left(1 + 4\cos^2\pi k_y a + 4\cos\pi k_y a \cdot \cos\pi k_x\sqrt{3}a\right)} \tag{2.4}$$

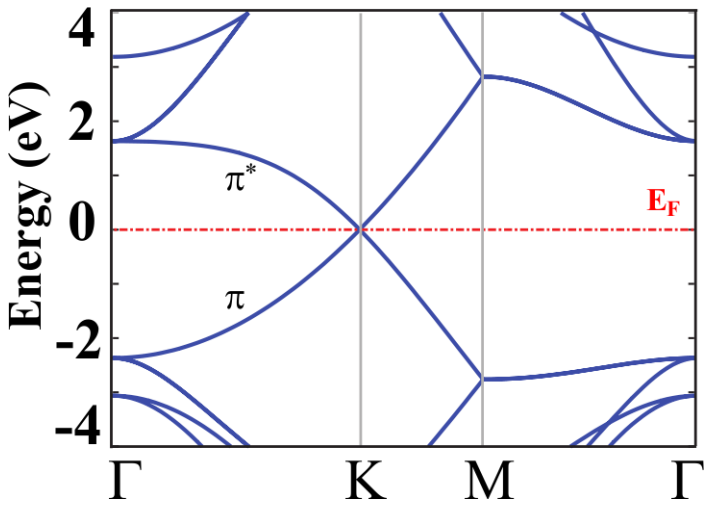

Figure 2.3: Band structure of the bare graphene calculated for the 2x2 unitcell.

[18].

with the nearest-neighbour-hopping energy $\gamma_0 \approx 2.8$ eV. $+$ and $-$ corresponds to the π^* and π energy bands, respectively. Figure 2.3 shows the band structure of 2D graphene. The energy dispersion around K is linear in momentum, $E = \hbar k v_f$, as if the relation for relativistic particles (like photons). In this case the role of the speed of light is given by the Fermi velocity $v_f \approx c/300$. Because of the linear spectrum, one can expect that particles in graphene behave differently from those in usual metals and semiconductors, where the energy spectrum can be approximated by a parabolic dispersion relation.

2.4 Graphene Nanoribbons

Graphene nanoribbons can be thought of as single wall CNTs cut along a line parallel to their axis and then unfolded into a planar geometry. There are two main shapes for graphene nanoribbon edges, namely armchair and zigzag edges. We can cut a graphene sheet in two different line with a difference of 30 ° in the axial direction between the two edge orientations to produce armchair and

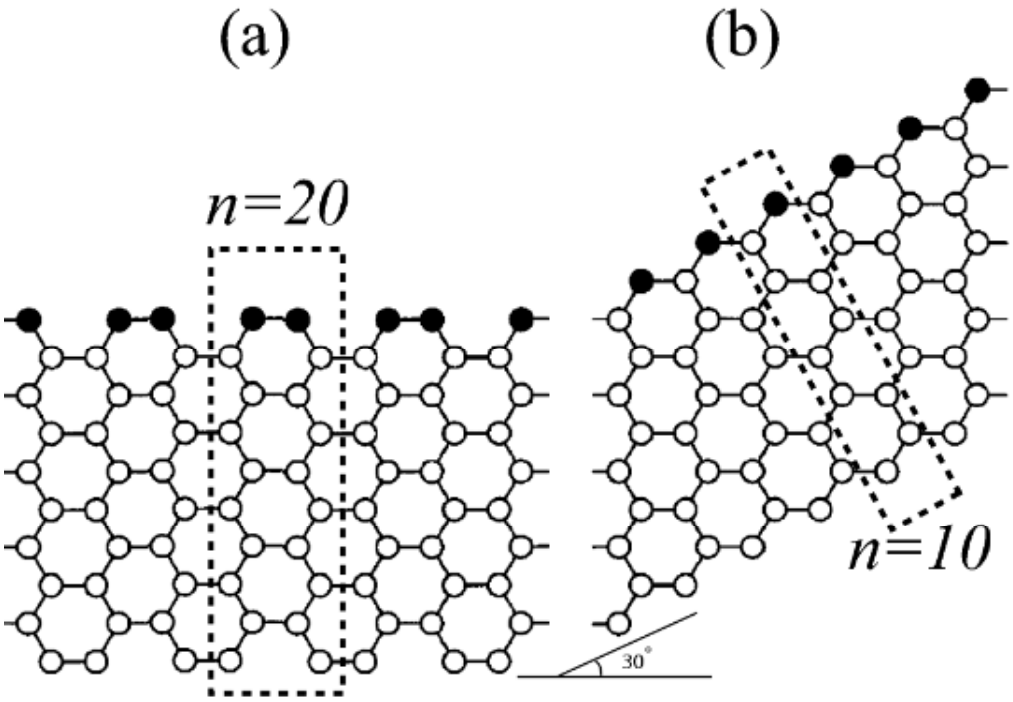

Figure 2.4: Graphene nanoribbons terminated by (a) armchair edges and (b) zigzag edges, indicated by filled circles. The unitcells are emphasized by dashed lines. The width "N" of ribbons are defined the number of carbon atoms in a unit cell.

zigzag graphene nanoribbons (see Fig. 2.4). If a ribbon is restricted by one of these edges, it is defined either as an armchair GNR (AGNR) or as a zigzag GNR (ZGNR) (see Fig. 2.4 (a &b).

The ribbon width can be defined by the number of carbon atoms in the primitive unit cell. Dashed rectangle in Fig. 2.4-a shows an armchair graphene nanoribbon containing 20 carbon atoms in its unitcell. This ribbon can be labelled as AGNR (20). On the other hand the ribbon in part (b) can be labelled as ZGNR (10) since it has zigzad shaped edges. Similar to the carbon nanotubes the width plays a crucial role on the electronic and magnetic properties of graphene nanoribbons.

Chapter 3

Density Functional Method

Our research performed on graphene based materials deals mostly with structural, electronic and magnetic properties. These properties can be obtained approximately by solving Schrödinger equation with periodic boundary conditions. The existence of a band gap in the band structure may give us some idea about the semiconducting or insulator behaviour of the system. Also the the broken degeneracy of spin-up and spin-down bands might give us information about the magnetization in the structure. Density Functional Method with Translational Periodicity can provide us structural, electronic and magnetic properties of graphene nanoribbons and this section will give a brief information about it.

Density functional theory has been very popular for calculations in solid state physics since the 1970s. In many cases DFT with the local-density approximation gives quite satisfactory results, for solid-state calculations, in comparison to experimental data at relatively low computational costs when compared to other ways of solving the quantum mechanical many-body problem. The success of density functional theory (DFT) not only encompasses standard bulk materials but also complex materials such as proteins and carbon nanotubes.

Although density functional theory has its conceptual roots in the Thomas-Fermi Approximation, DFT was put on a firm theoretical footing by the

Hohenberg-Kohn theorems in 1964 [28, 29] (after Pierre Hohenberg and Walter Kohn). The first of these demonstrates the existence of a one-to-one mapping between the ground state electron density and the ground state wavefunction of a many-particle system. Further, the second H-K theorem proves that the ground state density minimizes the total electronic energy of the system. This was almost 40 years after Schrodinger (1926) had published his pioneering paper marking the beginning of wave mechanics. Unfortunately in almost all cases except for the simple systems like He or H, this equation was too complex to allow a solution. DFT is an alternative approach to the theory of electronic structure, in which the electron density distribution $\rho(\mathbf{r})$ rather than many-electron wave function plays a central role. In the spirit of Thomas-Fermi theory [30, 31], it is suggested that a knowledge of the ground state density of $\rho(\mathbf{r})$ for any electronic system uniquely determines the system.

3.1 Hohenberg-Kohn Formulation

The first Hohenberg-Kohn theorem is an existence theorem, stating that the mapping exists. That is, the H-K theorems tell us that the electron density that minimizes the energy according to the true total energy functional describes all that can be known about the electronic structure. The Hohenberg-Kohn theorems relate to any system consisting of electrons moving under the influence of an external potential $\mathrm{V}(\mathbf{r})$. The Hohenberg-Kohn [28] formulation of DFT can be explained by two theorems:

Theorem 1: The external potential is univocally determined by the electronic density, except for a trivial additive constant.

Since $\rho(\mathbf{r})$ determines $\mathrm{V}(\mathbf{r})$, then this also determines the ground state wavefunction and gives the full Hamiltonian for the electronic system. So that $\rho(\mathbf{r})$ determines implicitly all properties derivable from H through the solution of the time-dependent Schrödinger equation.

Theorem 2: The minimal principle can be formulated in terms trial charge

densities, instead of trial wavefunctions.

The ground state energy E could be obtained by solving the Schrödinger equation directly or from the Rayleigh-Ritz minimal principle:

$$E = min\frac{\langle\widetilde{\Psi}|H|\widetilde{\Psi}\rangle}{\langle\widetilde{\Psi}|\widetilde{\Psi}\rangle} \tag{3.1}$$

Using $\widetilde{\rho}(\mathbf{r})$ instead of $\widetilde{\Psi}(\mathbf{r})$ was first presented in Hohenberg and Kohn. For a non-degenerate ground state, the minimum is attained when $\widetilde{\rho}(\mathbf{r})$ is the ground state density. And energy is given by the equation:

$$E_V[\widetilde{\rho}] = F[\widetilde{\rho}] + \int \widetilde{\rho}(\mathbf{r})V(\mathbf{r})d\mathbf{r} \tag{3.2}$$

with

$$F[\widetilde{\rho}] = \langle\Psi[\widetilde{\rho}]|\widehat{T} + \widehat{U}|\Psi[\widetilde{\rho}]\rangle \tag{3.3}$$

and $F[\widetilde{\rho}]$ requires no explicit knowledge of V($\mathbf{r}$).

These two theorems form the basis of the DFT. The main remaining error is due to inadequate representation of kinetic energy and it will be cured by representing Kohn-Sham equations.

3.2 Kohn-Sham Equations

The Kohn-Sham equations are a set of eigenvalue equations within density functional theory. Kohn and Sham introduced a method based on the Hohenberg-Kohn theorem that enables one to minimise the functional $E[\rho]$ by varying ρ over all densities containing N electrons. Thomas and Fermi gave a prescription for constructing the total energy in terms only of electronic density by using the expression for kinetic, exchange and correlation energies of the homogeneous electron gas to construct the same quantities for the inhomogeneous system [29]. This was the first time that the *Local Density Approximation* (LDA) was used. But this model is a severe shortcoming since this does not hold bound states and also the electronic structure is absent.

W.Kohn and L.Sham then proposed that the kinetic energy of the interacting electrons can be replaced with that of an equivalent non-interacting system which can be calculated easily. With this idea, the density matrix $\rho(r, r')$ of an interacting system can be written as sum of the spin up and spin down density matrices,

$$\rho_s(r, r') = \sum_{i=1}^{\infty} n_{i,s} \Phi_{i,s}(r) \Phi_{i,s}^*(r') \tag{3.4}$$

Where $n_{i,s}$ ar the occupation numbers of single particle orbitals, namely $\Phi_{i,s}(r)$. Now the kinetic energy term can be written as Eq.

$$T = \sum_{s=1}^{2} \sum_{i=1}^{\infty} n_{i,s} \langle \Phi_{i,s} | - \frac{\nabla^2}{2} | \Phi_{i,s} \rangle \tag{3.5}$$

This expression can be developed by considering that the Hamiltonian has no electron-electron interactions and thus eigenstates can now be expressed in the form of Slater determinant. By using this argument the density is written as

$$\rho(\mathbf{r}) = \sum_{s=1}^{2} \sum_{i=1}^{N_s} |\varphi_{i,s}(\mathbf{r})|^2 \tag{3.6}$$

and the kinetic term becomes

$$T[\rho] = \sum_{s=1}^{2} \sum_{i=1}^{N_s} \langle \varphi_{i,s} | - \frac{\nabla^2}{2} | \varphi_{i,s} \rangle \tag{3.7}$$

Now, we can write the total energy of the system in terms only of electronic density as follows,

$$E_{Kohn-Sham}[\rho] = T[\rho] + \int \rho(\mathbf{r}) v(\mathbf{r}) d\mathbf{r} + \frac{1}{2} \int \int \frac{\rho(\mathbf{r}) \rho(\mathbf{r}')}{|\mathbf{r} - \mathbf{r}'|} d\mathbf{r} d\mathbf{r}' + E_{XC}[\rho] \tag{3.8}$$

This equation is called the *Kohn-Sham Equations* After writing main equation, now the solution of the Kohn-Sham equations can be achieved by applying the same iterative procedure, in the same way of Hartree and Hartree-Fock equations. As a remark after all, in this approximation we have expressed the density functional in terms KS orbitals which minimize the kinetic energy under the fixed density constraint. In principle these orbitals are a mathematical object constructed in order to render the problem more tractable, and do not have a sense by themselves.

3.3 Exchange and Correlation

If we know the exact expression for the kinetic energy including correlation effects, then we can use the original definition of the exchange-correlation energy $E^0_{XC}[\rho]$ which does not contain kinetic contributions.

$$E^0_{XC}[\rho] = \frac{1}{2}\int\int \frac{\rho(r)\rho(r')}{\mid (r-r') \mid}[g(r,r')-1]drdr' \tag{3.9}$$

In this equation $E^0_{XC}[\rho]$ is the exchange-correlation energy without kinetic contributions. For writing the exchange-correlation energy $E_{XC}[\rho]$ as a function of ρ, we redefine Eq. 3.9 by considering the non-interacting expression for the kinetic energy $T_R[\rho]$ in the following way,

$$E_{XC}[\rho] = E^0_{XC}[\rho] + T[\rho] - T_R[\rho] \tag{3.10}$$

In this equation second term is interacting kinetic energy with correlation effects, while the last term corresponds to non-interacting kinetic energy. These two term can be considered as a modification to two-body correlation function $g(r,r')$ in Eq. 3.9. Updated two-body correlation function is now called as *average of pair correlation function*, and the exchange-correlation energy with kinetic contribution can be written as,

$$E_{XC}[\rho] = \frac{1}{2}\int\int \frac{\rho(r)\rho(r')}{\mid (r-r') \mid}[\widetilde{g}(r,r') - 1]drdr' \tag{3.11}$$

where $\widetilde{g}(r,r')$ can be expressed as follows,

$$\widetilde{g}(r,r') = 1 - \frac{\sum_\sigma \mid (\rho_\sigma(r,r') \mid^2)}{\rho(r)\rho(r')} + \widetilde{g_c(r,r')} \tag{3.12}$$

For further simplification for $E_{XC}[\rho]$, the exchange-correlation hole $\widetilde{g_{xc}(r,r')}$ is defined

$$\widetilde{g_{xc}(r,r')} = \rho(r')[\widetilde{g}(r,r') - 1] \tag{3.13}$$

so $E_{XC}[\rho]$ becomes,

$$E_{XC}[\rho] = \frac{1}{2}\int\int \frac{\rho(r)\widetilde{g_{xc}(r,r')}}{\mid (r-r') \mid}drdr' \tag{3.14}$$

After indicating fundamental equations of DFT theory now we can introduce to *Local Density Approximation* (LDA) and *Generalized Gradient Approximation* (GGA)

3.3.1 Local Density Approximation (LDA)

The local density approximation has been the most widely used approximation to handle exchange correlation energy. It has be proposed in the seminal paper by Kohn and Sham, but the philosophy was already present in Thomas-Fermi theory. In Local Density Approximation, the exchange-correlation energy of an electronic system is constructed by assuming that the exchange-correlation energy per electron at a point ρ in the electron gas, is equal to the exchange-correlation energy per electron in a homogeneous electron gas that has the same electron density at the point ρ. In fact LDA based on two main approximations, (1) The

pair function is approximated by that of the homogeneous electron gas density $\rho(r)$ corrected by the density ratio $\rho(r)/\rho(r')$ to compansate the fact that the LDA exchange-correlation hole is now centered at r instead of r' (2) The LDA exchange-correlation hole interacts with the electronic density at r, and is centered at r. But as we know that the real exchange-correlation hole is actually centered at r' instead r.

3.3.2 Generalized Gradient Approximation (GGA)

Although the the LDA was the universal choice for ab-initio calculations on amorphous systems, there were well known problems with the approximation: (1) First of all in the local density approximation the optical gap is always poorly estimated (normally underestimated). Of course, this does not affect ground state properties like charge density, total energy and forces, but it serious problem for calculations of conduction states, as for example in the case of transport or optical properties.(2) In strongly (electronically) inhomogeneous systems such as SiO, the basic assumption of weak spatial variation of the charge density is not well satisfied, hence the LDA has difficulty. (3) The LDA assumes that the system is paramagnetic; the local spin density approximation [32] (LSDA) (in which a separate "spin up" and "spin down" density functional is used) is useful for systems with unpaired spins, as for example a half filled state at the Fermi level.

Several workers, but especially Perdew [33], have worked on next step to the LDA: inclusion of effects proportional to the gradient of the charge density. Recent improvements along these ways are called *Generalized Gradient Approximations* (GGA), it seems that these have led to significant improvements in SiO [34], and intermolecular binding in water is better described with GGA than in the LDA. In some ways the GGA has been disappointing; on very precise measurements on molecules the results have been mixed. But overall, the GGA seems to be an improvement over the conventional LDA.

In GGA exchange-correlation energy can be written as follows,

$$E_{XC}[\rho] = \int \rho(\mathbf{r})\epsilon_{XC}[\rho(\mathbf{r})]d\mathbf{r} + \int F_{XC}[\rho(\mathbf{r}, \nabla\rho(\mathbf{r}))]d\mathbf{r} \tag{3.15}$$

where the function F_{XC} is asked to satisfy the formal conditions.

GGA approximation improves binding energies, atomic energies, bond lengths and bond angles when compared the ones obtained by LDA. In our calculations, we used the GGA approximation [35].

3.4 Periodic Supercells

By using the represented formalisms observables of many-body systems can be transformed into single particle equivalents. However, there still remains two difficulties: A wave function must be calculated for each of the electrons in the system and the basis set required to expand each wave function is infinite since they extend over the entire solid. For periodic systems both problems can be handled by Bloch‘s theorem [36].

3.4.1 Bloch‘s Theorem

Bloch theorem states that in a periodic solid each electronic wave function can be written as:

$$\Psi_i(\mathbf{r}) = u_i(\mathbf{r})e^{i\mathbf{kr}} \tag{3.16}$$

where u_k has the period of crystal lattice with $u_k(\mathbf{r}) = u_k(\mathbf{r}+\mathbf{T})$. This part can be expanded using a basis set consisting of reciprocal lattice vectors of the crystal.

$$u_i(\mathbf{r}) = \sum_G a_{k,G}e^{i(\mathbf{G})\mathbf{r}} \tag{3.17}$$

Therefore each electronic wave function can be written as a sum of plane waves

$$\Psi_i(\mathbf{r}) = \sum_G a_{i,k+G}e^{i(\mathbf{k}+\mathbf{G})\mathbf{r}} \tag{3.18}$$

3.4.2 k-point Sampling

Electronic states are only allowed at a set of **k**-points determined by boundary conditions. The density of allowed **k**-points are proportional to the volume of the cell. The occupied states at each **k**-point contribute to the electronic potential in the bulk solid, so that in principle, an finite number of calculations are needed to compute this potential. However, the electronic wave functions at **k**-points that are very close to each other, will be almost identical. Hence, a single **k**-point will be sufficient to represent the wave functions over a particular region of **k**-space. There are several methods which calculate the electronic states at special **k** points in the Brillouin zone [37]. Using these methods one can obtain an accurate approximation for the electronic potential and total energy at a small number of **k**-points. The magnitude of any error can be reduced by using a denser set **k**-points.

3.4.3 Plane-wave Basis Sets

According to Bloch‘s theorem, the electronic wave functions at each **k**-point can be extended in terms of a discrete plane-wave basis set. Infinite number of plane-waves are needed to perform such expansion. However, the coefficients for the plane waves with small kinetic energy $(\hbar^2/2m)|\mathbf{k}+\mathbf{G}|^2$ are more important than those with large kinetic energy. Thus some particular cutoff energy can be determined to include finite number of **k**-points. The truncation of the plane-wave basis set at a finite cutoff energy will lead to an error in computed energy. However, by increasing the cutoff energy the magnitude of the error can be reduced. We carried out convergence tests with respect to the cut-off energy or the number of plane waves used in the expansion of Bloch states.

3.4.4 Plane-wave Representation of Kohn-Sham Equations

When plane waves are used as a basis set, the Kohn-Sham(KS) [29] equations assume a particularly simple form. In this form, the kinetic energy is diagonal and potentials are described in terms of their Fourier transforms. Solution proceeds by diagonalization of the Hamiltonian matrix. The size of the matrix is determined by the choice of cutoff energy, and will be very large for systems that contain both valence and core electrons. This is a severe problem, but it can be overcome by considering pseudopotential approximation. Large Hamiltonian matrices are diagonalized using iterative methods, which do not require large computer memory.

Chapter 4

Results

4.1 Introduction and Motivation

Graphene nanoribbons (GNRs) are just geometrically terminated forms of perfect 2D graphene where the electrons are confined in two direction and free to move in third direction. At this point, let us define that our graphene nanoribbon lies on the x-y plane. The width is defined along the y-axis and the length is defined along the x-axis as seen in Fig. 4.1 (a).

The homogeneous nanoribbons are the structures that have the same width throughout the ribbon length. The formation of vacancies in AGNRs is not a rare situation [46, 47] and have remarkable effects on electronic and magnetic properties. On the other hand, heterogeneous nanoribbons can be obtained by differing the ribbon width and composition at junctions. Fig. 4.1 (a), (b), (c) shows the forms of graphene ribbon structures that we have investigated in this thesis. Extensive first principles calculations have been performed on various heterostructres and quite interesting results have been obtained. Initial investigations of uniform GNRs ((Fig. 4.1-a)) have been performed for a proper understanding of modified structures (Fig. 4.1 (b), (c)).

We predicted superlattice structures of graphene nanoribbons of alternating

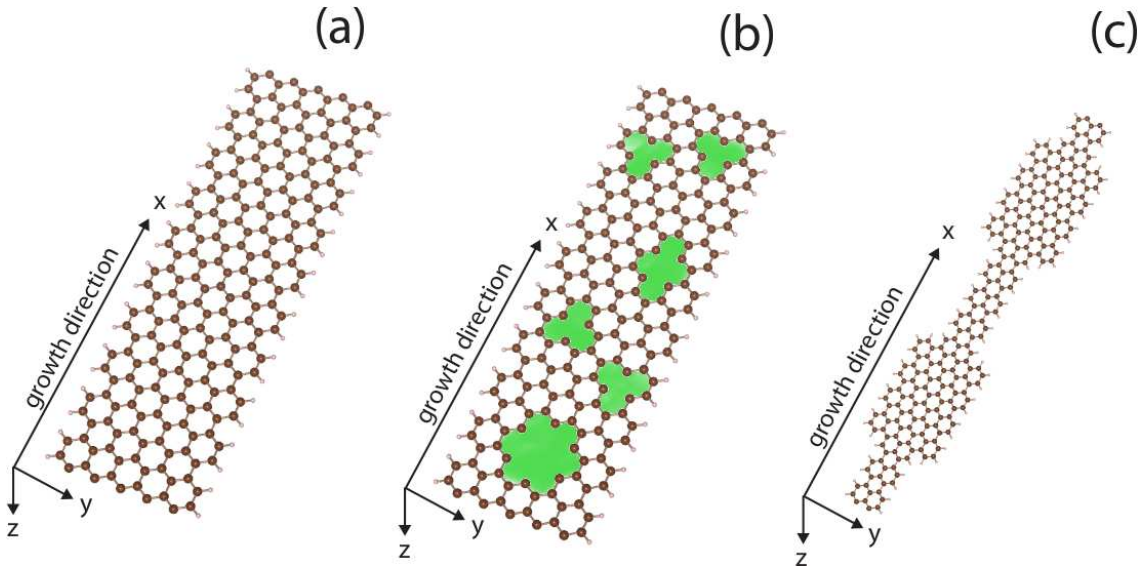

Figure 4.1: The ribbons are periodic along the x-axis. The width is defined along y-axis. (a) An armchair graphene nanoribbon without any vacancy and size modulation. (b) An armchair graphene nanoribbon having several defects in its structure with different types and positions. (c) A superlattice of graphene nanoribbon which was formed with a combination of wide and narrow AGNR.

widths leading to confined states. We presented an extensive discussion of various kinds of superlattice geometries and corresponding electronic structure. In particular, we found that the periodically repeating heterostructures of BN/Graphene armchair nanoribbon result in multiple quantum well structures with minibands and confined states. This is a 1D analog of 2D, pseudomorphic or commensurate semiconductor superlattices. These superlattices have been subject of very active study since 1980s and have led to the discovery of integer and fractional quantum Hall effects, quantum ballistic transport with quantized conductance and other exceptional properties of electrons in lower dimensionality. In addition, several novel devices fabricated from AlAs/GaAs or Si/Ge quantum structures have displayed outstanding device performance.

Our study performed on defected GNRs have also shown that the band gap and magnetic state of any armchair or zigzag nanoribbons can be modified by single or multiple vacancies (holes). The effects of these defects depend on their symmetry, repeating periodicity and positions. When combined with various properties of nanoribbons these results can initiate a number of interesting applications.

We believe that our results are important for further studies, since the graphene ribbons can now be produced with precision having widths sub 10 nm [12] and nanodevices can be fabricated thereof [38].

4.2 Method of Calculations

Here we present specific parameters used in the calculations related with graphene ribbons using the Viena ab initio Simulation package (VASP) [39]. We have performed first-principles plane-wave calculations within density functional theory DFT using ultrasoft pseudopotentials. The exchange correlation potential has been approximated by generalized gradient approximation GGA using PW91 functional. For partial occupancies, we use the Methfessel-Paxton smearing method. The adopted smearing width is 0.1 eV for the atomic relaxation and

0.01 for the accurate band structure analysis and density of state calculations. All structures have been treated within a supercell geometry using the periodic boundary conditions. Calculations have been performed in momentum space by using periodically repeating tetragonal supercell with the lattice constants , $a_s = b_s = 10\ \mathring{A}$ whereby interaction of nearest neighbors in the y and z directions are negligible. Convergence tests have been performed with respect to the energy cut-off and number of k-points. A plane-wave basis set with kinetic energy of up to 500 eV has been used. 35-1-1 k-points in the Brioullin zone are used in the k-space within the Monkhorst-Pack scheme [40] . Ribbons are built from the perfect graphite geometry with an initial C-C distance of 1.42 Å. All atomic positions and lattice constants are optimized by using the conjugate gradient method where total energy and calculated Hellmann-Feynman atomic forces are minimized. The criterion of convergence for energy is chosen to be $10^{-}5$ eV between two ionic steps, and the maximum force allowed on each atom is 0.05 eV/ Å.

4.3 Armchair and Zigzag Graphene Nanoribbons

The geometry of armchair nanoribbons and their bond lengths are illustrated on Fig. 4.2 (a). We have investigated the bond length deviations of nanoribbons from 2-D perfect graphene after ionic relaxation. It was seen that the final structures didn't change considerably from the ideal honeycomb pattern with C-C length of 1.42 $\mathring{A}$, and H terminations with C-H length of 1.1 Å. Fig.- 4.2 shows the bond lengths of several graphene ribbons. C-C bond lengths close to the edges are relatively narrower ($\approx 14\%$) especially for bare ribbons which have dangling bonds on the edges. The minimum bond length is around 1.23 $\mathring{A}$ for bare-AGNR(10). The terminations of those edges with hydrogen atoms release the narrow bonds and make them similar to the bulk bonds which are around 1.43 Å. On the other hand narrower AGNRs have slightly wider unit cell lengths and the length of unit cell decreases gradually with the number of atoms in each cell as seen in Fig. 4.2 (b).

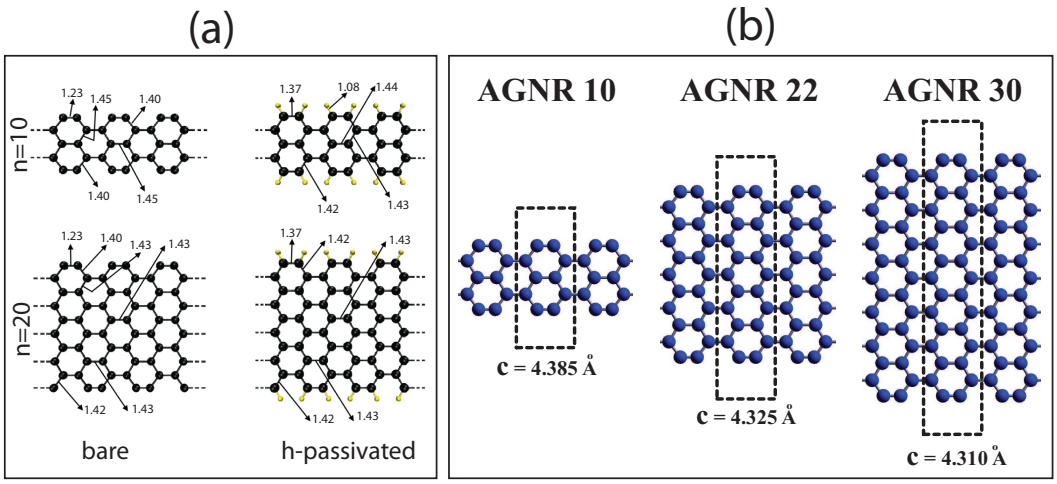

Figure 4.2: Deviations of bond lengths (a) and unit cell length (b) for some of graphene nanoribbons. (a) The bare and hydrogen terminated ribbons are shown on the left and right, respectively. The distances are in units of $\AA$ and small balls corresponds to H atoms. (b) Deviation of unit cell length for some AGNRs. The structure gets narrower with the increase in the width of the ribbon.

4.4 Width Dependence of Graphene Nanoribbons and Hydrogen Passivation

We have defined the width of our nanoribbons in Section 2.4. Similar to the carbon nanotubes, which are just rolled up structures of graphene nanoribbons, the band gaps of AGNRs are inversely proportional to the ribbon width "w". This variation is understood more easily if we categorize the ribbon width into three distinct families such as N = $6m-2$, $6m$, $6m+2$ (m being an integer) where N is the number of carbon atoms in primitive unit cell. All AGNR(N) are semiconductors and their band gap, E_g, vary with N. It is small for N=$6m-2$, but from $6m$ to $6m+2$ it increases and passing through a maximum it becomes again small at the next minimum corresponding to $6m-2$. As E_g oscillates with N its value decreases eventually to zero as $N \rightarrow \infty$ which is case for perfect 2D graphene. On the other hand, band gaps of ZGNRs decrease steadily with the width of the ribbon. The variation of energy band gaps of bare and hydrogenated ribbons for AGNRs and ZGNRs as a function of N is plotted in Fig. 4.3. Our results are

in good agreement with some other first principles calculations obtained by LDA method [41, 43]. These calculations will be useful for our further results that we will an in following sections.

The band gap values of bare AGNR(10) and AGNR(14) shown in Fig. 4.4 (a) and (b) are significantly different and are of 0.44 and 1.10 eV, respectively. Two different kinds of bands are distinguished by their charge density plots. These are bands of states having charge density uniformly distributed across the ribbon and those of edge states having their charge localized at both edges of the ribbon. Owing to the interaction between two edges of the narrow ribbon, the bands of edge states split. Upon termination of the carbon dangling bonds by hydrogen atom, the edge states disappear, and the energy band gaps are modified. While hydrogen terminated AGNR(10) has a narrow band gap of 0.39 eV, hydrogen terminated AGNR(14) has a wide band gap of 1.57 eV. The $6m-2$ family which has the smallest band gap have been predicted to have 0 eV band gap by some theoretical calculations [44, 45]. But all of our DFT calculations show the existence of a band gap.

4.5 Mechanical Properties of Graphene Nanoribbons

In this section, we explore the mechanical properties of graphene nanoribbons. The stability and electro-mechanical properties of nanoribbons are crucial for their possible use in future nanoelectronics. The rate of change of the band gap with strain, $\epsilon = \Delta c/c$ (Δc being the change of lattice constant under uniaxial stress along the $x-$axis.) in Fig. 4.5(a), i.e. $\partial E_g/\partial\epsilon$ is significant and its sign changes with N. We also calculated the variation of total energy with strain, ϵ and its second derivative with respect to strain, $\kappa^{'} = \partial^2 E_T/\partial\epsilon^2$ (in units of eV/cell). Results summarized in Fig. 4.5 (b) and (c) indicate that graphene nanoribbons are quasi 1D, stiff materials. For example, $\kappa^{'}$ =351 eV/cell for ZGNR(6). Interestingly, ZGNR(N) appear to be stiffer than AGNR(n) for the same n. These values can be compared with $\kappa^{'}$=127 eV/cell calculated for linear

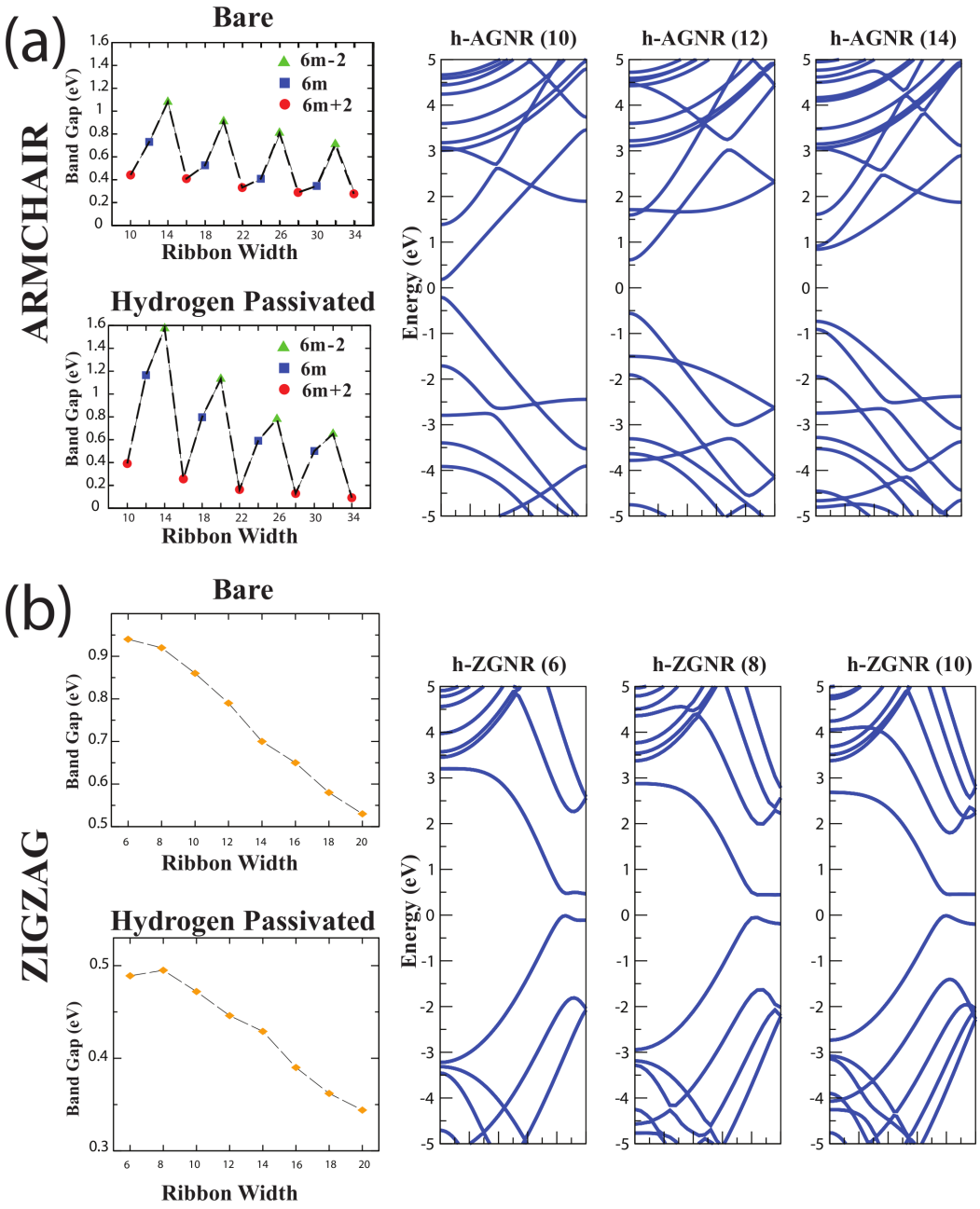

Figure 4.3: Calculated variation of band gaps of AGNR(N) ZGNR(N) as a function of ribbon width N for (a) armchair and (b) zigzag ribbons. The band structure of some of ribbons are shown on the right.

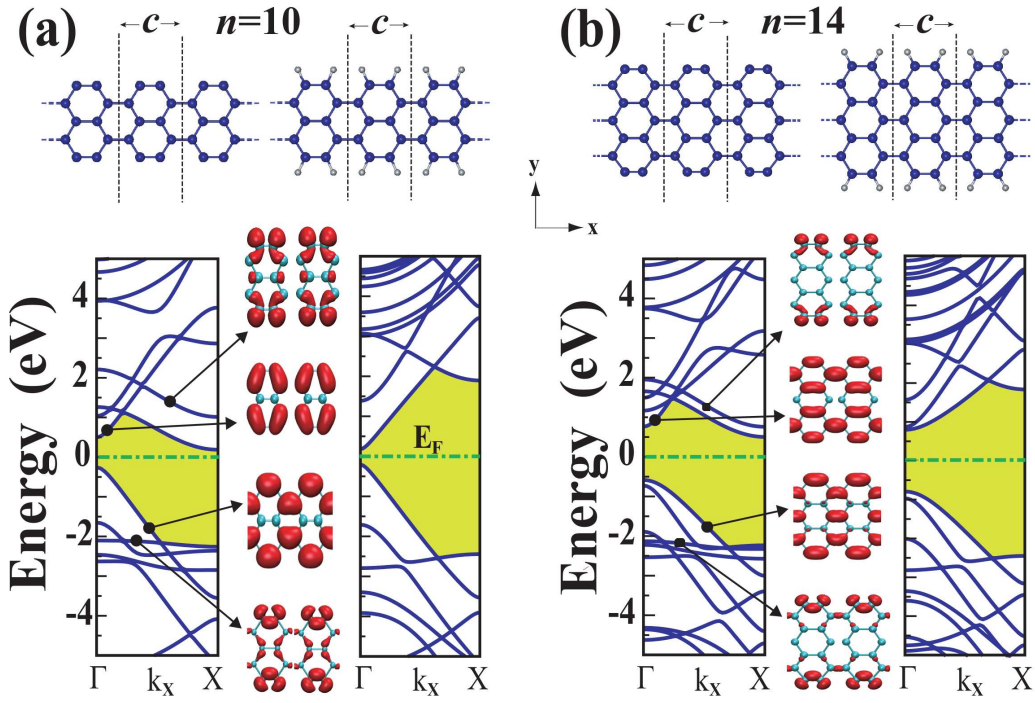

Figure 4.4: (a) Bare and hydrogen terminated AGNR(10): Atomic geometry, electronic band structure and isosurface charge densities of edge and "uniform" states. The primitive unit cell is delineated with dashed lines and includes N=10 carbon atoms. Carbon and hydrogen atoms are shown by large and small balls. (b) Same for AGNR(14).

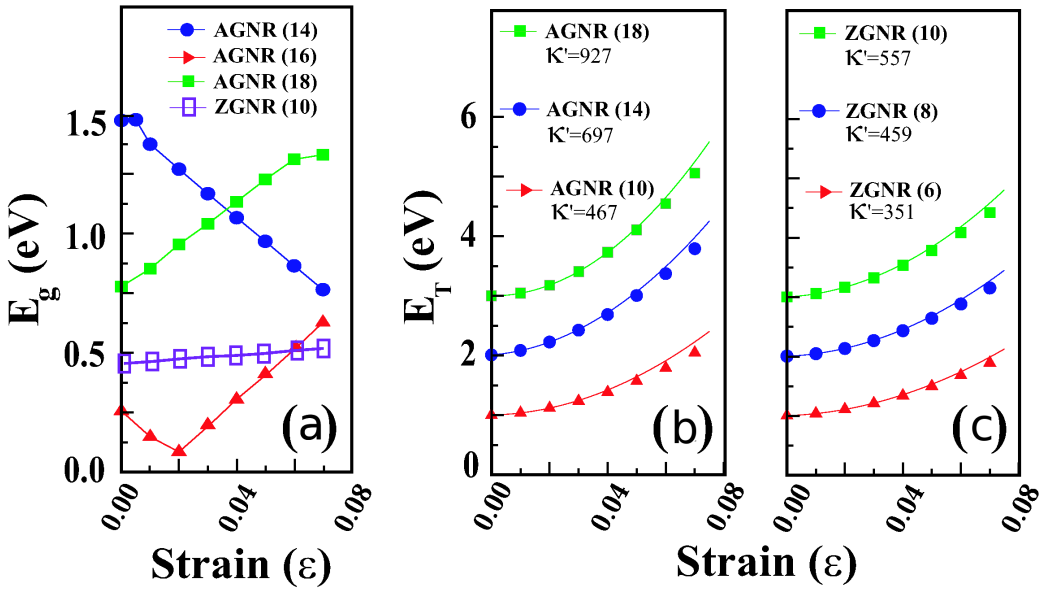

Figure 4.5: (a) Variation of band gaps E_g of AGNR and ZGNR, with the tensile strain, ϵ. (b) Variation of the total energy of AGNR with ϵ and its second derivative with respect to ϵ, i.e. $\kappa^{'}$ [eV/cell]. (c) Same as (d) for ZGNR. All data in this figure are calculated using first-principles methods.

carbon chain and confirm the robustness of heterostructures.

4.6 Monitoring of band gap and magnetic state of graphene nanoribbons through vacancies

Recent studies have shown that vacancies created on 2D graphene by high-energy electron or ion irradiation can induce magnetism in a system consisting of only *sp*-electrons[48, 49]. It has been argued that Stoner magnetism with high T_C originates from the spin-polarized extended states induced by the vacancy defects, while RKKY coupling is suppressed. These effects of defects on 1D semiconducting graphene nanoribbons should be more complex and interesting, because their band gap, magnetic state and symmetry are expected to intervene.

A hole can be created when carbon atoms at the corners of any hexagon of an armchair ribbon are removed and subsequently remaining six two-fold coordinated carbon atoms are terminated with hydrogen atoms. Fig. 4.6 shows that the electronic structure of AGNR(34) is strongly modified by such a hole placed at the center of the ribbon. The hole (see Fig. 4.6 (b)) repeats itself at each supercell which comprises six primitive cells corresponding to a repeat period of l=6. This ribbon having a periodic hole (or defect) is specified as AGNR(N;l) and has non-magnetic ground state. Despite large separation of periodic defect which hinders their direct coupling such a strong modification of the band gap is somehow unexpected. However, it is an indirect effect and occurs since the itinerant states of band edges are modified by the defect. At the end, the direct band gap at the Γ-point has widened from 0.09 eV to 0.40 eV because a defect situated at the center of the ribbon. In contrast, the band gap of bare AGNR(38), which is normally larger than that of bare AGNR(34), is reduced if the same hole is introduced at its center (see Fig. 4.7 (b)). In addition, localized states around the defect have formed flat bands near the edge of valence andconduction bands because of their reduced coupling.

It is even more interesting that the effect of hexagonal defect is strongly dependent on its position relative to the both edges of the nanoribbon as depicted in Fig. 4.7. As shown in Fig. 4.7 (b), the changes in band gap depend on N of AGNR (in the family specified as $6m + q$, q being -2, 0 and +2) as well as on the position of the hole. As shown in Fig. 4.7 (b), the effects of defect decrease with increasing repeat periodicity l.

We found that larger holes with different geometry and rotation symmetry can result in diverse electronic structure and confined states. It should be noted that a repeating hole can also modify the mechanical properties. For example, the stiffness of a ribbon is reduced by the presence of a hole. The force constant, $\kappa = \partial^2 E_T/\partial c^2$ (c being the lattice constant) calculated for AGNR(34;6) with a hole at its center (κ = 6.03 eV/Å) is found to be smaller than that without a hole κ =7.50 eV/Å).

Another defect, a divacancy created in AGNR(22) can cause to a dramatic

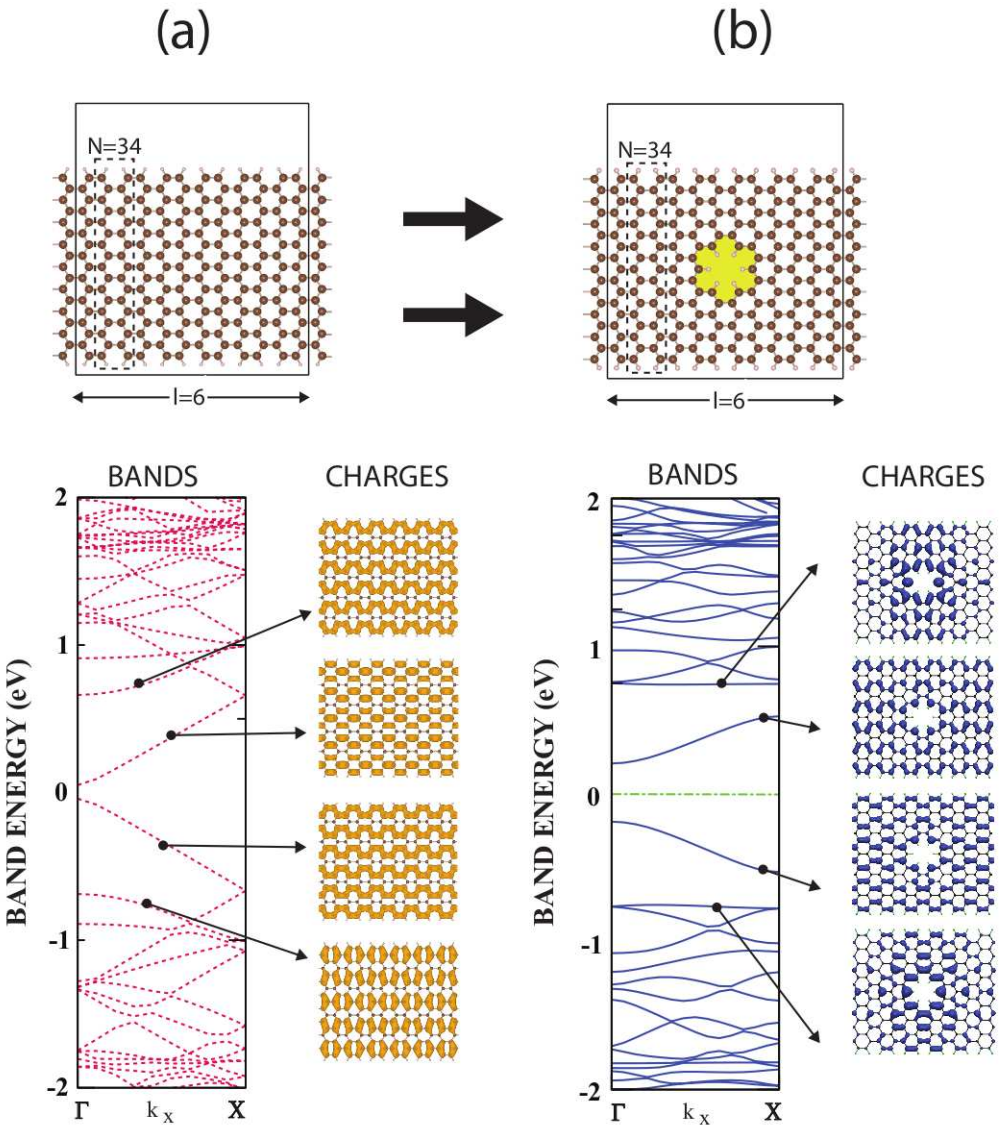

Figure 4.6: (a) Atomic configuration and band structure of AGNR(N=34,l=6) without a hole consisting of six carbon vacancies. Charge density isosurfaces of selected states are given on the right. (b) Atomic configuration, band structure and charge density isosurfaces of selected states of AGNR(N=34,l=6) with a hole consisting of six carbon vacancies. Carbon atoms, which have coordination number lower than 3 are terminated by hydrogen atoms.

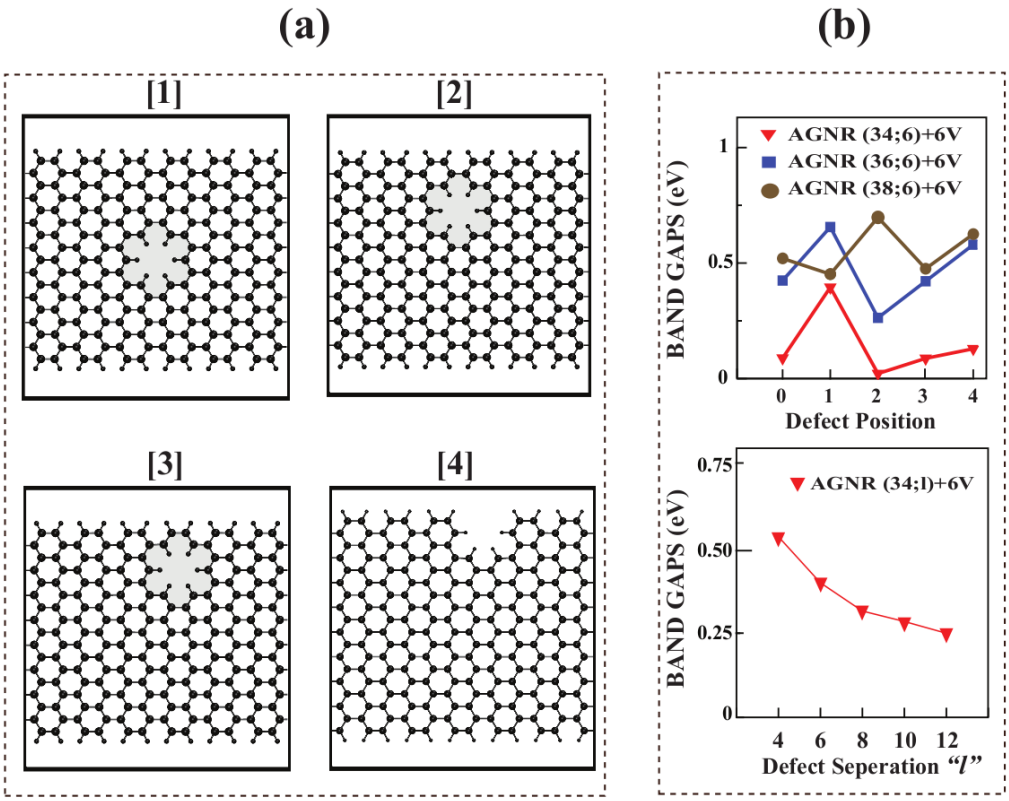

Figure 4.7: (a) Four distinct positions of a hole in the ribbon are indicated by numerals. (b) Variations of band gaps of AGNR(N,l) with the position of defect and with repeat periodicity, l. "V" stands for the vacancy.

change in the electronic state of the ribbon when it is repeated with the periodicity of l=5. Such an armchair ribbon is specified as AGNR(22;5). The divacancy first relaxes and forms an eight fold ring of carbon atoms which is adjacent to six hexagons and two pentagons. In Fig. 4.8 (a) we see that the non-magnetic and semiconducting AGNR(22) with band gap of E_G=0.18 eV becomes a non-magnetic metal, since a flat band derived from the defect occurs below the top of the valance band edge and causes to a metallic state.

The effect of a single carbon vacancy becomes even more interesting. A single vacancy created in AGNR(22) is relaxed and the three-fold rotation symmetry is broken due to Jahn-Teller distortion. At the end, a nine-sided ring forms adjacent to a pentagon as shown in Fig. 4.8 (b). Owing to the spin-polarization of the sp^2-dangling bond on the two-fold coordinated carbon atom and adjacent orbitals at the defect site the system obtains an unbalanced spin. In fact, the difference of total charge density corresponding to states of different spin states, i.e. $\Delta\rho_T = \rho_T^{\uparrow} - \rho_T^{\downarrow}$ is non-zero and exhibits a distribution shown in Fig. 4.8 (b). Because of unbalanced spin, AGNR(22;5) gains a net magnetic moment of μ=1 μ_B per cell. This attributes a magnetic state to the nanoribbon, which was nonmagnetic otherwise.

Furthermore, the spin degeneracy of some bands related with this defect is broken and spin-up and spin-down bands are split. The dispersive, non-magnetic band at the edge of the valence band becomes partially emptied, since its electrons are transferred to the flat spin bands below. Eventually, the semiconducting ribbon becomes metallic.

Not only armchair, but also zigzag nanoribbons are strongly affected by defects due to single and multiple vacancies. The magnetic state and energy band structure of these ribbons depend on the type and geometry of the defects. In Fig. 4.9 (a)-(c), the effect of a defect generated from the single vacancy with a repeat periodicity of l=8 is examined in ZGNR(14;8) for three different positions. The total energy is 0.53 eV lowered when the defect is situated at the edge rather than at the center of the ribbon.

ZGNR(14;8) has a net magnetic moment of μ=1.94 μ_B when the defect is

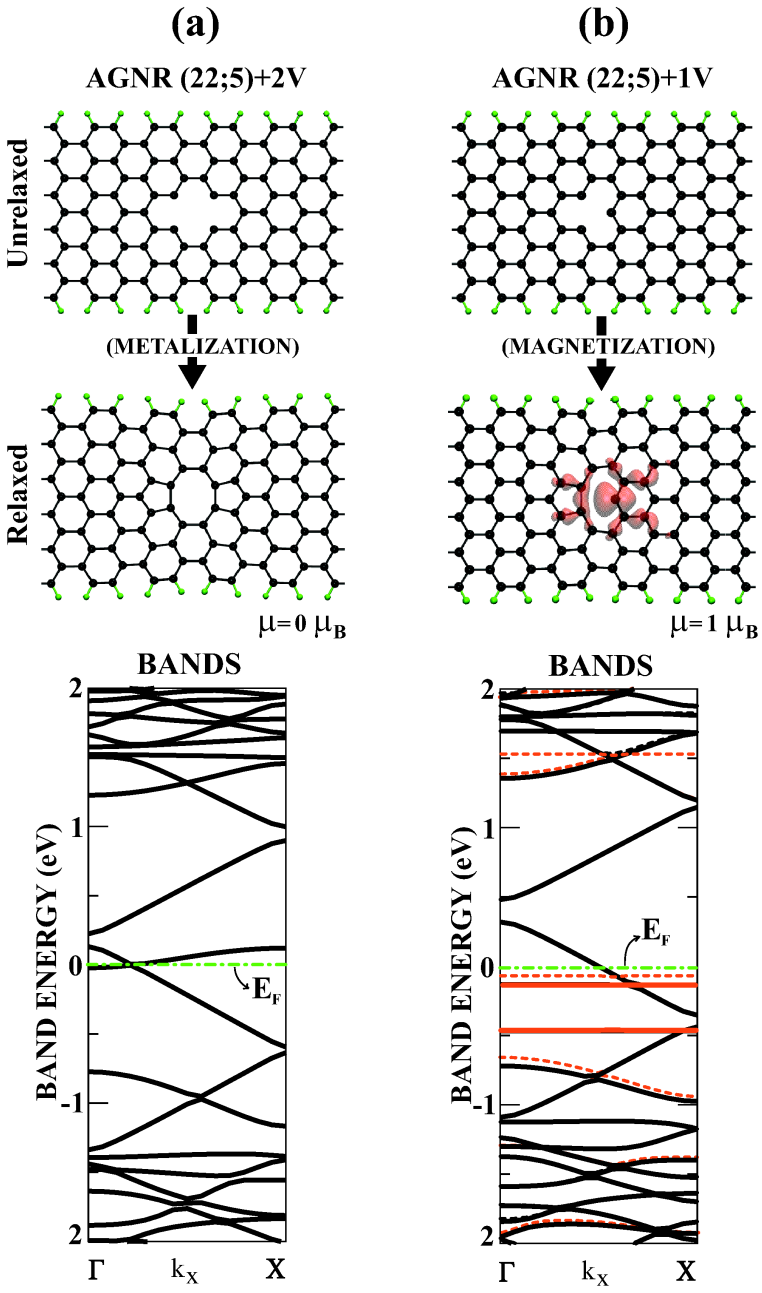

Figure 4.8: (a) Metallization of the semiconducting AGNR(22) by the formation of divacancies with repeat period of l=5. (b) Magnetization of the non-magnetic AGNR(22) by a defect due to the single carbon atom vacancy with the same repeat periodicity. Solid (blue) and dashed (red) lines are for spin-up and spin-down bands; solid (black) lines are nonmagnetic bands.

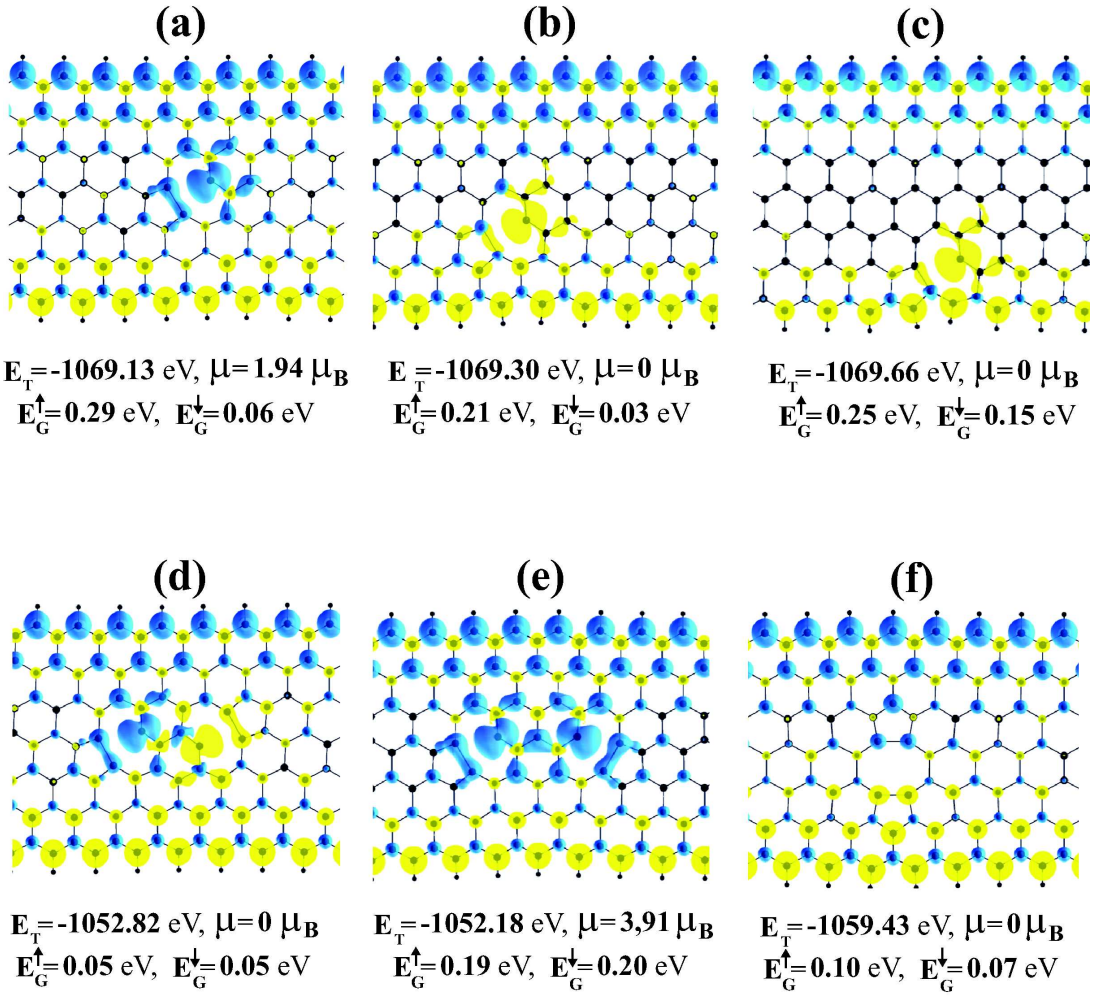

Figure 4.9: Vacancy and divacancy formation in an antiferromagnetic semiconductor ZGNR(14) with repeat period of l=8. Calculated total energy, E_T (in eV/cell), net magnetic moment, μ (in Bohr magneton μ_B/cell), band gap between spin-up(down) conduction and valence bands, $E_G^{\uparrow(\downarrow)}$) are shown for each case.

situated at the center of the ribbon and hence its antiferromagnetic ground state has changed to ferrimagnetic state through the magnetic moment of the single vacancy. Otherwise, μ becomes zero, when the position of the defect deviates from the center. For example, in Fig. 4.9 (b) and (c) the sum of the magnetic moments of the edge states is not zero, but the net magnetic moment per unit cell becomes zero only after the spins of the defect is added. Even if the net magnetic moment μ=0, ZGNR(14,8) does not have an antiferromagnetic ground state due to the presence of single vacancy. The edge states, each normally having equal but opposite magnetic moments, become ferrimagnetic when a defect is introduced. The total magnetic moment of the supercell vanish only after the magnetic moment of defect has been taken into account. Since the spin-degeneracy has been broken, one can define $E_G^{\uparrow}$ and $E_G^{\downarrow}$ for majority and minority spin states. Not only the magnetic state, but also the band gap of zigzag ribbons in Fig. 4.9 are affected by the symmetry and the position of the defect relative to edges. In Fig. 4.9 (d)-(f) two defects associated with two separated vacancy and a defect associated with a relaxed divacancy exhibit similar behaviors.

An important issue to be addressed is the breakdown of Lieb's theorem[50] for those zigzag ribbons. According to Lieb's theorem, the net magnetic moment per cell is determined with the difference in the number of atoms belonging to different sublattices, and it shall be either μ=1 μ_B or 2 μ_B for the cases in Fig. 4.9. None of the cases in Fig. 4.9 is in agreement with Lieb's theorem. Here one can consider two features, which may be responsible for this discrepancy. First is the strong Jahn-Teller distortion and relaxation of carbon atoms at the close proximity of the defect. As a result some dangling sp^2-bonds reconstructed to form C-C covalent bonds. The lowering of the total energy, a driving force for such reconstruction, is as high as 0.5-0.6 eV/cell. Second is the interaction with the magnetic edge states, which becomes effective for narrow ZGNRs.

4.7 Superlattice Structures of Graphene Nanoribbons: confined states

After investigating the homogeneous nanoribbons whose band gaps change with their width, we constructed periodically repeating heterojunctions made of different widths. Our studies based on extensive first-principles calculations have shown that periodically repeating heterojunctions made of graphene ribbons of different widths (and hence different band gaps) can form multiple quantum well structures. These superlattices are unique since both size and energy band gap, even the magnetic ground state for specific structures vary periodically in direct space. As a consequence, in addition to the propagating states, specific states are localized in certain regions. Localization increases and turns to a complete confinement when the extent of the ribbons with different widths increases. Widths, lengths, chirality of constituent ribbons and the symmetry of the junction provide variables to engineer quantum structures with novel electronic and transport properties.In particular, finite-size quantum structures can be combined to design various devices, such as resonant tunnelling double barrier (RTDB) or asymmetric Aharonov-Bohm loops. Once these devices are functionalized with transition metal atoms, the broken spin-degeneracy of states with energies $E_n(\mathbf{k},\uparrow)$ and $E_n(\mathbf{k},\downarrow)$, can be used for spintronics applications [17] .

The superlattices that we consider in this section are labelled as AGSL(n_1,n_2;s_1,s_2) which are made by the segments of AGNR(n_1) and AGNR(n_2). Here, s_1 and s_2 specify the length of segments in terms of their numbers of unit cells . Fig. 4.10 (a) shows a superlattice AGSL(10,14;3,3). It is a combination of AGNR(10) and AGNR(14) to form a periodic AGNR(10)/AGNR(14) junction.

4.7.1 AGSL(10,14;s_1,s_2) Family

Hydrogen passivated AGNR(10) is a direct band gap material with a band gap of 0.39 eV. AGNR(14) is also a direct band gap material with a band gap of 1.57 eV. The combined heterostructure with a symmetric junction has a band

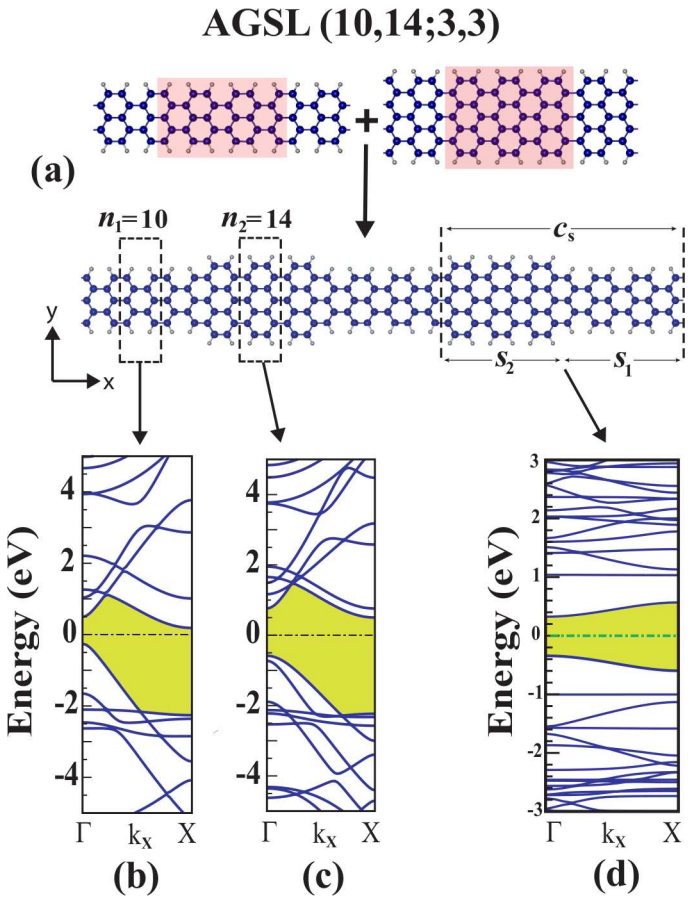

Figure 4.10: Formation of a graphene nanoribbon heterostructres AGSL(10,14;3,3). (a) Atomic structure of AGSL($n_1 = 10$, $n_2 = 14$; $s_1 = 3$, $s_2 = 3$). The superlattice unit cell and primitive unit cell of each segment are delineated. (below) Band structures of constituent segments (b)-(c) and superlattice (d) with band gaps of 0.39, 1.57 and 0.65 eV respectively.

gap of 0.65 eV. The band structure of constituent segments and the supercell is shown in Fig. 4.10. Upon junction formation, dramatic changes occur in the band structure of this superlattice. Highest valance and lowest conduction bands are dispersive, but bands below and above the dispersive ones are simply flat. These flat states are also represented by sharp peaks in density of states (DOS) plots (see Fig. 4.11 (a)). The isosurface charge density plots distinguish the different characters of these bands. For example, as highest valance band states propagate across the superlattice, the states of the second (flat) band are confined to the wider part of AGSL(10,14;3,3) consisting of AGNR(14) segment. These flat band states are identified as *confined* states.

Normally, a particular state, which is propagating in one region (or segment) is confined if it cannot find a matching state in the adjacent region having the same energy. For a superlattice of small n_1 or n_2, spacings between energy levels are significant and hence localization of states in one of the regions is more frequent. This argument, which is relevant for superlattices of long constituent segments, may not be valid for short segments (or small s_1 and s_2). The confined states have been treated earlier in commensurate or pseudomorphic junctions of two different semiconductors, which form a periodically repeating superlattice structure [51]. These superlattices have grown layer by layer and form a sharp lattice matched interface. Owing to the band discontinuities at the interface, they behave as if a multiple quantum well structure obeying the Effective Mass Theory. Two dimensional conduction band electrons (valence band holes) confined to the well display a number of electronic and optical properties. In the present case, both the band gap and the size (width) of the graphene ribbon are periodically modulated in direct space and carriers are one dimensional. On the other hand the atomic arrangement and lattice constants at both sides of the junction are identical; the hetero character concerns only the width of the ribbons at different sides.

Electronic and transport properties of graphene multiple quantum well structures can be controlled by a number of structural parameters. In addition to n_1, n_2, s_1, s_2, symmetry of the junction, $\Delta n = n_2 - n_1$, even-odd disparity of $n_1/2$ and $n_2/2$, type of the interface between two different ribbons and the shape of the superlattice (namely sharp rectangular or smooth wavy) influence the properties.

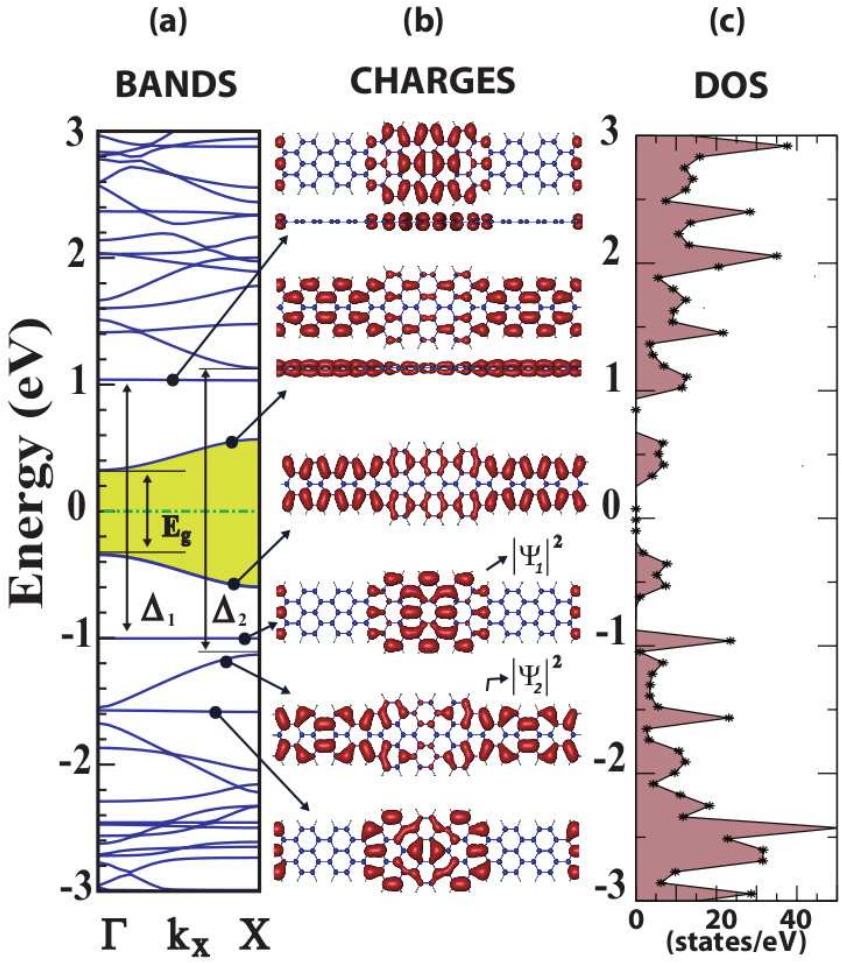

Figure 4.11: (a) Band structure of AGSL(10,14;3,3) with flat bands corresponding to confined states. (b) Isosurface charge density of propagating and confined states. (c) Density of States (DOS) of AGSL(10,14;3,3) with sharp peaks corresponding to confined states.

As shown in Fig. 4.12 superlattice band gaps decrease as s_1 increase from 3 to 8. This is a clear evidence for quantum size effect. In terms of the weight of the states in the segment s_2, i.e. $\int_{s_2} |\Psi(\mathbf{r})|^2 d\mathbf{r}$, we see that the confinement of states increases with increasing s_1; but it disappears for s_1=s_2=1 (see Fig. 4.17 (a)). Confinement increases with increasing $s_1 = s_2$ and hence with increasing barrier width, since the penetration of states into the barrier decreases). For example, AGSL(10,14;s_1,s_2) has E_g=0.66,0.48,0.38,0.32,0.27 eV for s_2=3 and s_1=3,4,5,6,7, respectively. Conversely, E_g=0.72,079,0.83,0.84 eV for s_1=3 and s_2=4,5,6,7, respectively. On the other hand, the energy of the flat-band states confined to s_2 and their weight are practically independent of s_1.

4.7.2 AGSL(10,18;s_1,s_2) Family

In this section, we investigate the effects of changing n_1 from 14 to 18. Two nanoribbons containing 10 and 18 carbon atoms in their unit cell are merged. Note that AGNRs can be constructed by using two different unit cells (i.e. those consisting of complete hexagons or of incomplete hexagons). A junction with complete hexagons is preferred in order to prevent a lonely carbon atom at the interface. For AGSL with reflection symmetry the narrow region is made by unit-cells having complete or incomplete hexagons depending on whether $(n_2-n_1)/4$ is an even or odd number, respectively. Variation of $\Delta n = n_1 - n_2$ results in a wide variety of electronic structures. For example, in contrast to AGSL(10,14;3,3) the highest valence and lowest conduction bands of AGSL(10,18;3,3) are flat bands with E_g=0.70 eV; dispersive bands occur as second valence and conduction band having a gap of 1.18 eV between them. Fig. 4.14 shows the band structure of AGSL(10,18;3,3) with flat bands corresponding to confined states. Since the first valance and conduction are confined in wider region of the structure, this ribbon can act as a resonant tunneling double barrier diode. The narrow regions act as a barrier and wider region as a quantum well. As seen from Fig. 4.14 we have complete confinement of charges for some of states in wider region. On the other hand, the states which are mostly confined in narrower region can penetrate to the wider regions. The variation of s_1 for AGSL(10,18;s_1,s_2) family have similar

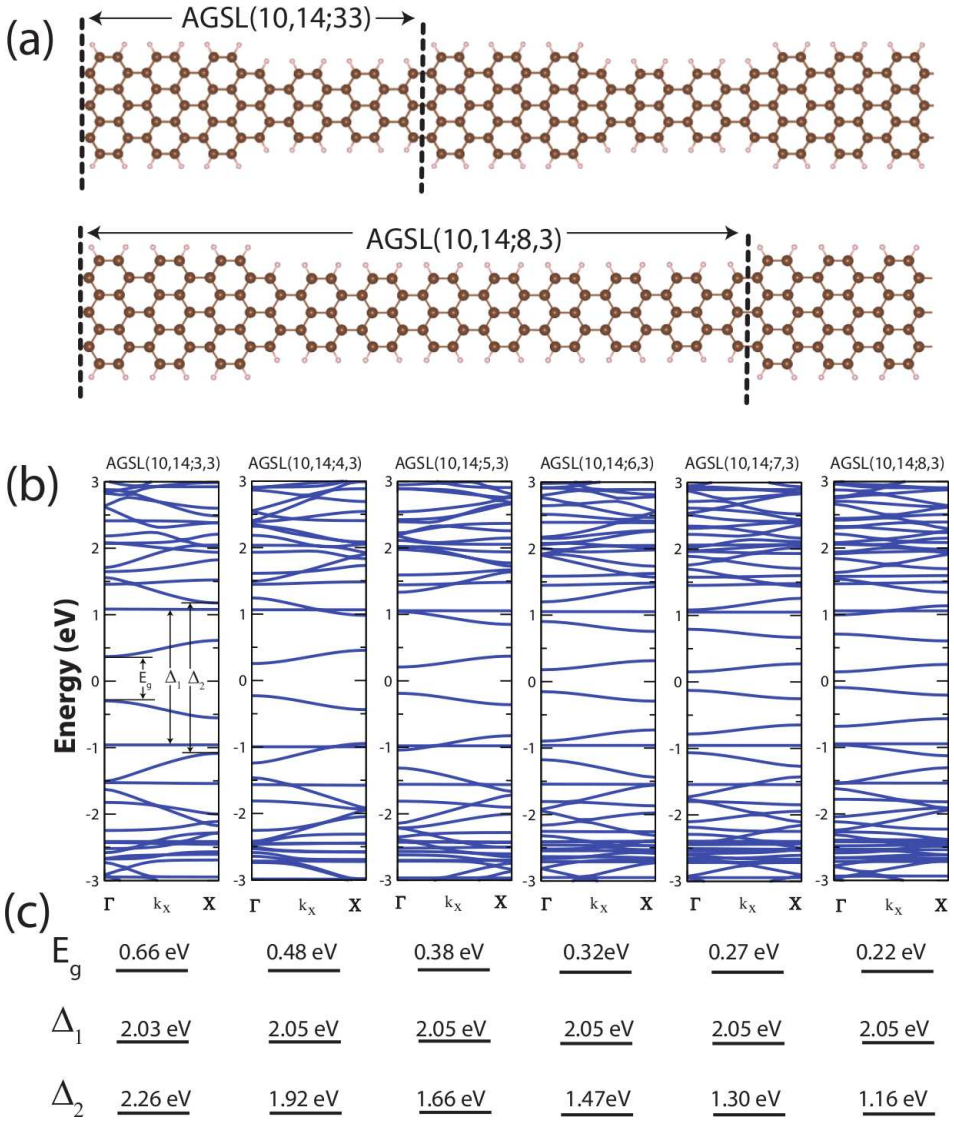

Figure 4.12: (a) The variation of narrower region (s_1) of AGSL(10,14;3,3) from 3 to 8 while the wider part remains the same. (b) The variation of band structures. (c) The numerical values for energy gaps E_g, Δ_1, Δ_2. E_g is the actual band gap of the structure which comes from a dispersive state. Δ_1 is the band gap of highest localized state while Δ_2 is the band gap for the next dispersive state. As seen above, the energy of the flat-band states (Δ_1) confined to s_2 and their weight are practically independent of s_1.

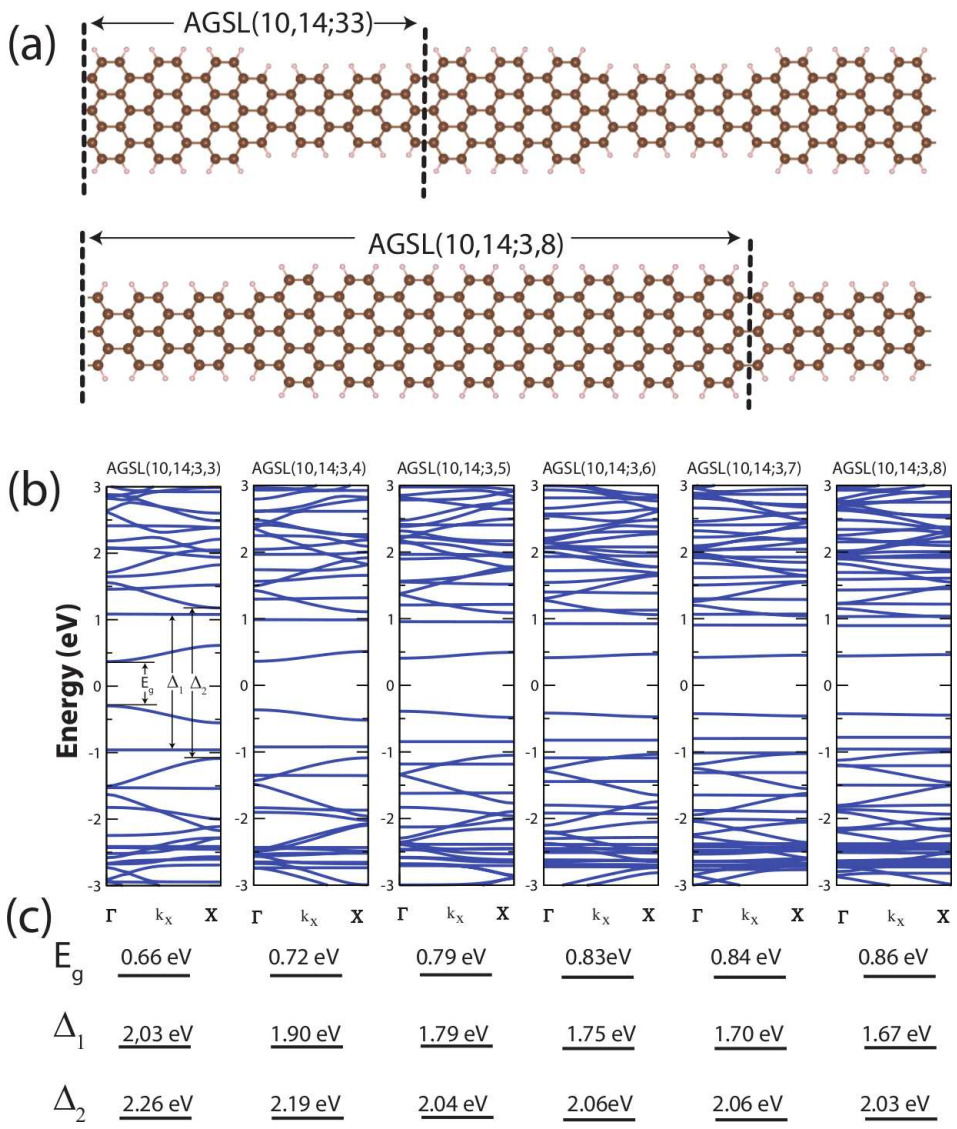

Figure 4.13: (a) The variation of wider region (s_2) of AGSL(10,14;3,3) from 3 to 8 while the narrower part remains the same. (b) The variation of band structures. (c) E_g, Δ_1, Δ_2. E_g is the actual band gap of the structure which comes from a dispersive state. Δ_1 is the band gap of highest localized state while Δ_2 is the band gap for the next dispersive state. In this case, E_g slightly changes while Δ_1 decreases due to quantum size effect.

consequences to the AGSL(10,14;s_1,s_2). Again we see that the confinement of states increase with increasing s_1. As shown in Fig. 4.15 superlattice band gaps decrease as s_1 increase from 3 to 7. On the other hand, the energy of the flat-band states confined to s_2 and their weight are practically independent of s_1. As shown in Fig. 4.16 the band gaps of localized conductance and valance states decrease with the increase in s_2. These findings reveal that charge confinement in size modulated graphene nanoribbons is closely related with structural parameters of heterostructure.

4.7.3 Other Structures

Figure 4.17 shows some of other structures. Large amount of electrical properties can be obtained by differing n_1, n_2, s_1, s_2, the symmetry of the junction, $\Delta n = n_2 - n_1$, even-odd disparity of $n_1/2$ and $n_2/2$ and the type of the interface between two different ribbons. For example figure 4.17 (a) shows the analysis of AGSL(10,14;1,1). It contains only one unit cell of AGNR(10) and AGNR(14) segments. As seen from the figure, the charge confinement that we investigated in section 4.7.1 is completely destroyed. The flat states in band structure and sharp peaks in DOS are missing. All states near Fermi level are propagating throughout the ribbon.

Figure 4.17 (b) shows the antisymmetric superlattice. Again it consists of AGNR(10) and AGNR(14) segments. One of the edges is straight while the other one is alternating. Interstingly, the charge confinement still survives. This is one of the evidences for the robustness of charge confinement in size modulated graphene nanoribbons.

The superlattice shown in Fig. 4.17 (c) is a member of another family which is wider than AGSL(10,14;3,3). The charge confinement is still observed. But the positions of completely localized states are further from Fermi level than AGSL(10,14;3,3). Fig. 4.17 (d) shows n_2=13 form of the structure shown in part (c). With the richness of structural parameters of armchair graphene nanoribbon heterostructres one can find a desired geometry for the fabrication of novel

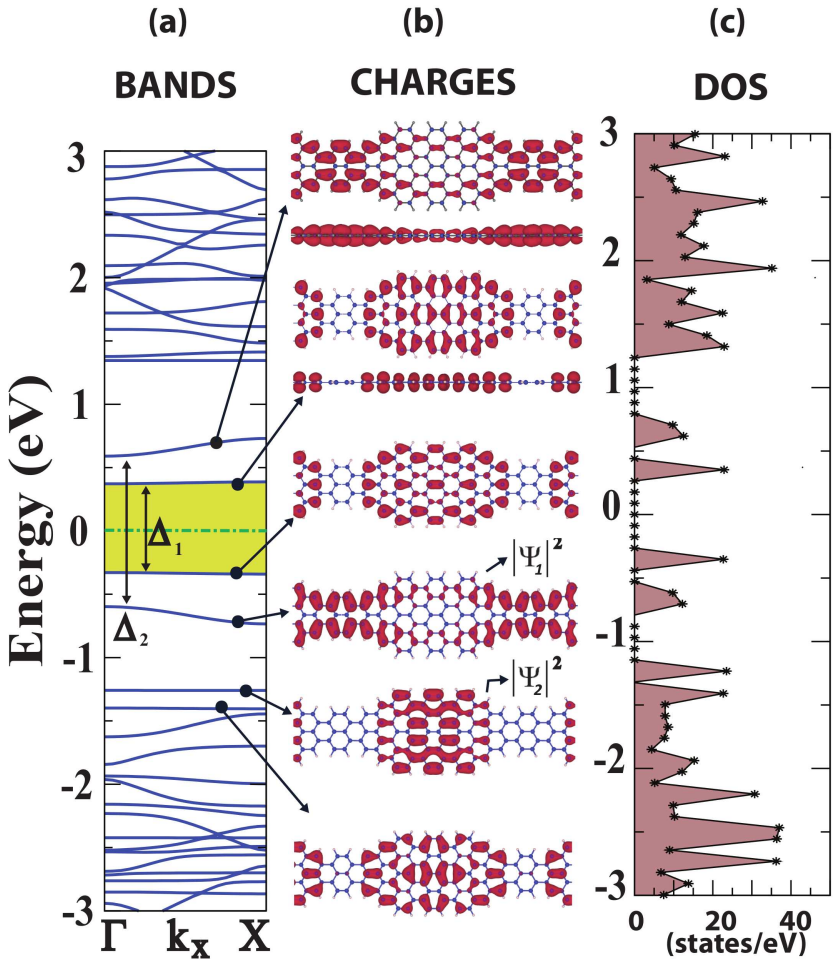

Figure 4.14: (a) Band structure of AGSL(10,18;3,3) with flat bands corresponding to confined states. (b) Isosurface charge density of propagating and confined states. (c) Density of states (DOS) of AGSL(10,18;3,3) with sharp peaks corresponding to confined states.

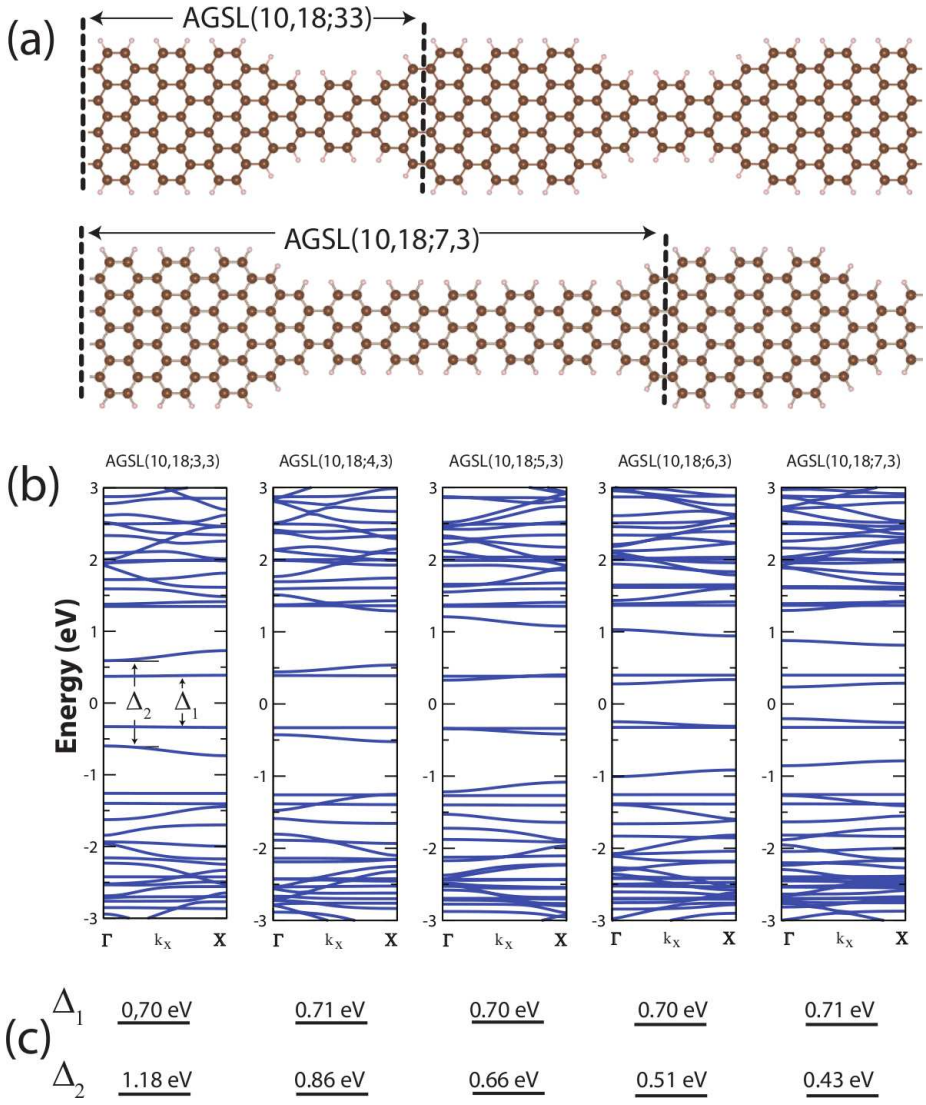

Figure 4.15: (a) The variation of narrower region (s_1) of AGSL(10,18;3,3) from 3 to 7 while the wider part remains the same. (b) The variation of band structures. (c) The numerical values for energy gaps Δ_1, Δ_2. Δ_1 is the band gap of highest valance and first conductance state while Δ_2 is the band gap for the next dispersive states. As seen above, the energy of the flat-band states (Δ_1) confined to s_2 and their weight are practically independent of s_1.

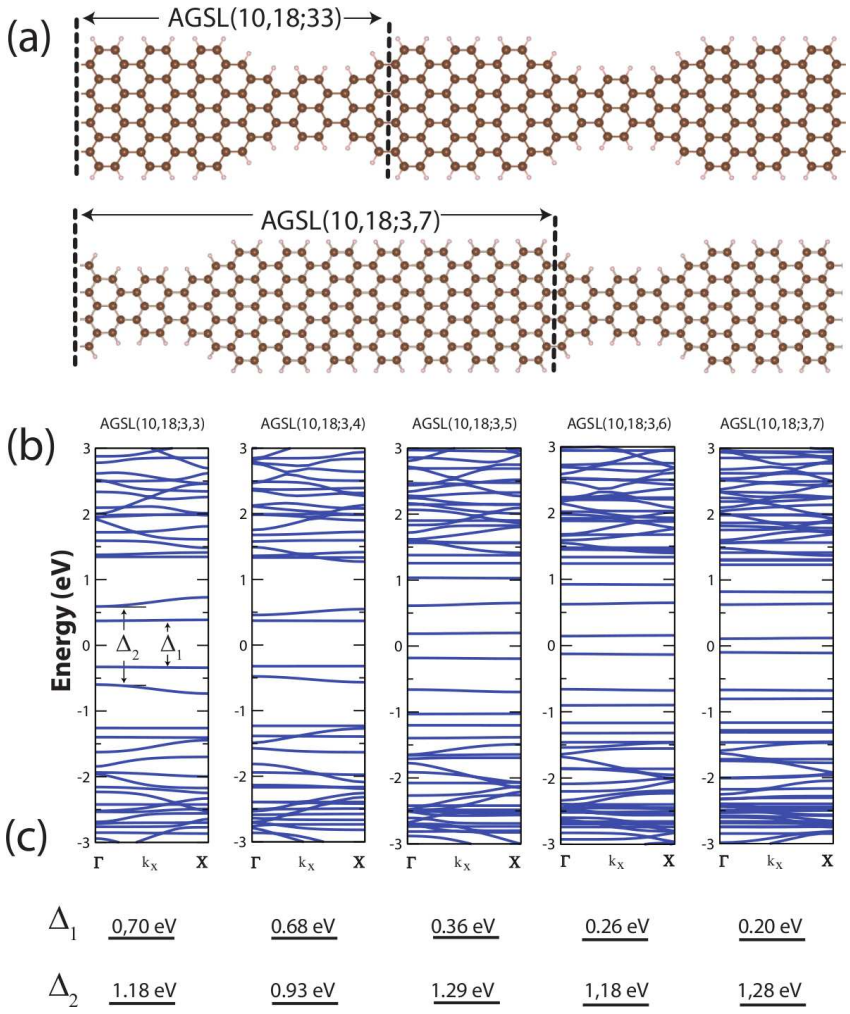

Figure 4.16: (a) The variation of wider region (s_2) of AGSL(10,18;3,3) from 3 to 7 while the narrower part remains the same. (b) The variation of band structures. (c) The numerical values for energy gaps Δ_1, Δ_2. Δ_1 is the band gap of highest valance and first conductance state while Δ_2 is the band gap for the next dispersive states. In this case, Δ_2 oscillates while Δ_1 decreases due to quantum size effect.

nanodevices.

4.7.4 Mechanical Properties of Superlattices

The rate of change of band gaps with strain, $\epsilon = \Delta c/c$ (Δc being the change of lattice constant under uniaxial stress along the $x-$axis.) of nanoribbon superlattice structures is also a notable feature, which may be interesting for future stress-gauge device applications. In Fig. 4.18 (f) and Fig. 4.18 (g) we present our results for the variation of E_g and other relevant gaps of the nanoribbon superlattice AGSL(10,14;3,3) and also its constituent AGNR's for the sake of comparison. Strong dependence on ϵ is impressive. That these superlattice structures are quasi 1D stiff materials is shown by the variations of their total energies E_T with respect to ϵ in Fig. 4.18 (h). The force constant of the superlattice calculated by $\kappa_S = \partial^2 E_T/\partial c^2$ is in good agreement with the equivalent force constant $\kappa_{eq,SL} = (s_1/\kappa_{n_1} + s_2 + \kappa_{n_2})^{-1}$ calculated in terms of the force constants of the constituent nanoribbons κ_{n_1} and κ_{n_2}. This shows that elastic properties of superlattices comply with Hooke's law for small $\Delta n = n_2 - n_1$. It is also interesting to note that the force constant of AGNR(14,3), $\kappa = 11.57$ eV/$\mathring{A}$, can be compared with that of carbon linear chain $\kappa = 26.24$ eV/$\mathring{A}$.

4.7.5 Compositional Modulation of Heterostructres

The confined states have been treated earlier in commensurate or pseudomorphic junctions of two different semiconductors, which form a periodically repeating 2D superlattice structure [51]. These superlattices have grown layer by layer and formed a sharp lattice matched interface. Owing to the band discontinuities at the interface, they behave as if a multiple quantum well structure according to the Effective Mass Theory [52]. Two dimensional conduction band electrons (valence band holes) confined to the wells have displayed a number of electronic and optical properties [53, 54, 55, 56]. In Fig. 4.19, we present a 1D analog of the 2D semiconductor superlattices through compositional modulated nanoribbons. BN honeycomb ribbon and graphene ribbon of the same width are lattice matched

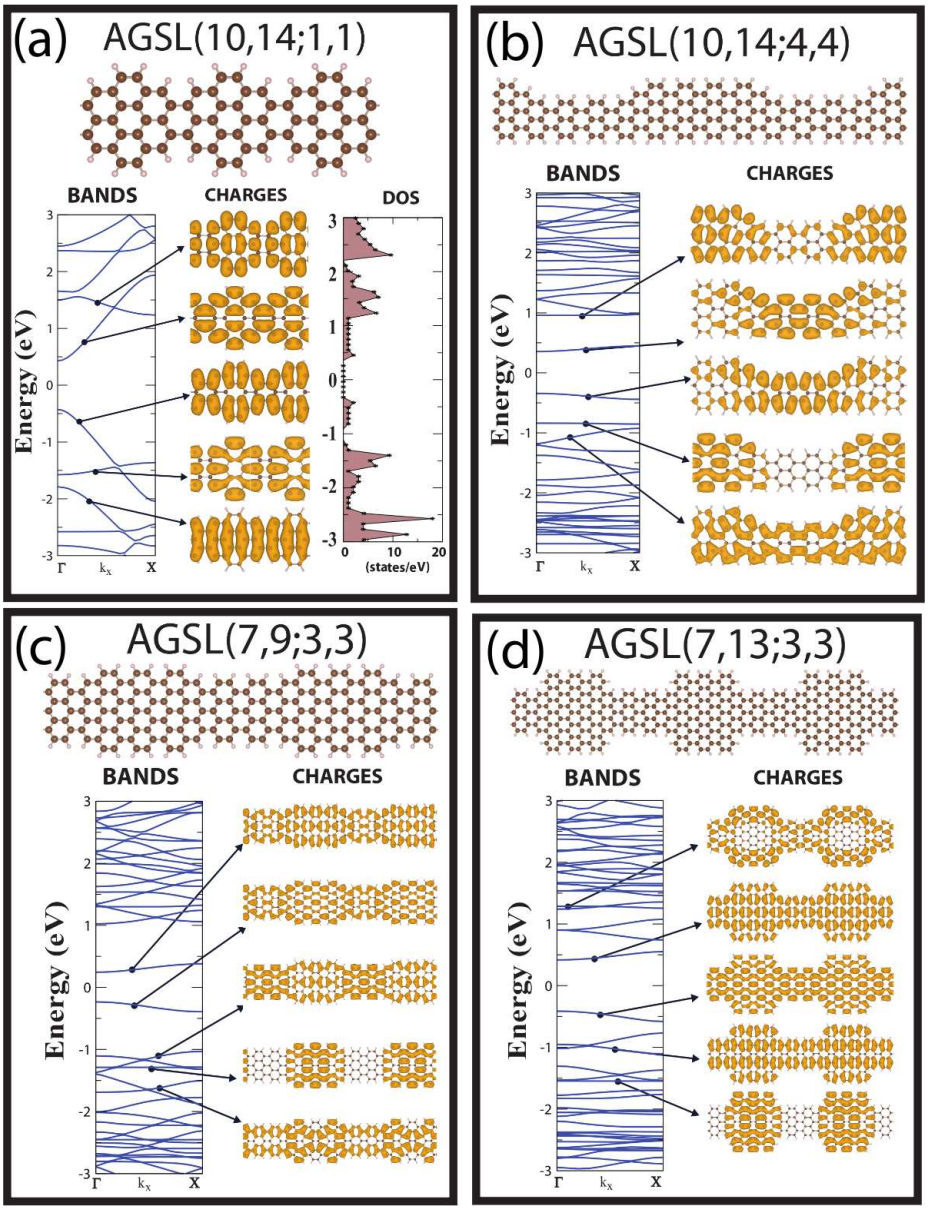

Figure 4.17: Other superlattice structures made by varying the geometrical parameters. (a) is an example of very small superlattice where the charge confinement is destroyed. (b) is an example of antisymmetric superlattice where charge confinement still survives. (c) & (d) are some of other structures.

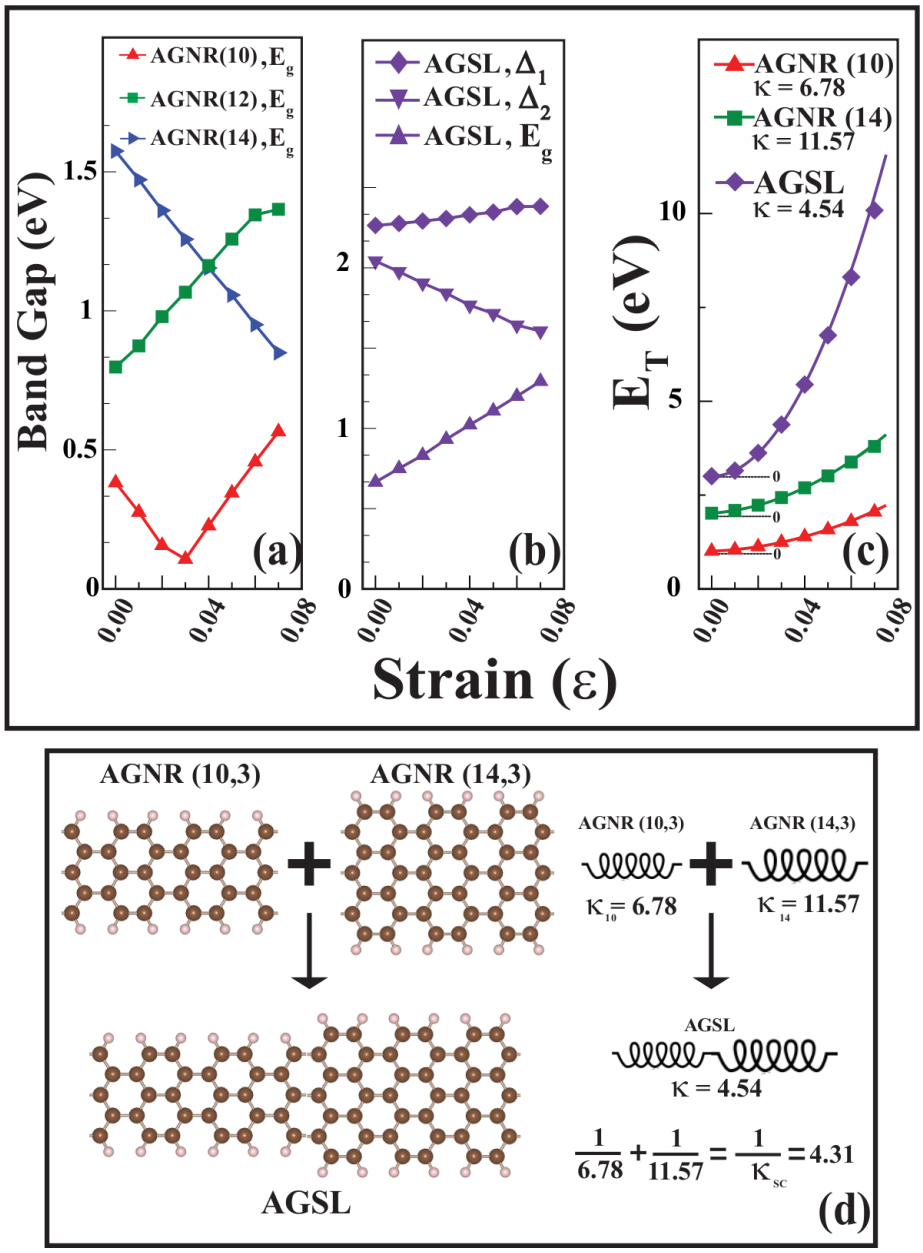

Figure 4.18: (a) Variation of band gaps E_g of constituent AGNR's with the tensile strain ϵ. (b) Same for the nanoribbon superlattice AGSL(10,14:3,3). (c) Variation of the total energy E_T with respect to ϵ, and the force constant, κ_{SC} [in $eV/\mathring{A}$] for AGSL(10,14;3,3) and its constituent nanoribbons. (d) Illustration of Hooke's law. When two nanoribbons with different force constant, κ , is merged. The resulting structure's force constant,κ_{SC}, can be estimated according to Hooke's law. In our case, the calculated κ value (4.31 $eV/\mathring{A}$) is slightly less than the real value (4.54 $eV/\mathring{A}$)

and can form superlattices with multiple quantum well structure with confined states. We considered a periodic junction of the segment of armchair BN ribbon with n_1=18 and s_1=3 to the segment of armchair graphene with n_2=18 and s_2=3 to form a superlattice structure. While periodic BN and graphene ribbons by themselves have band gaps of $\sim$5 eV and 0.8 eV, respectively, the band gap of BN/AGNR(18) is only 0.8 eV indicating a normal (type-I) band alignment. Under these circumstances, a state propagating in one segment becomes confined if its energy coincides with the band gap of the adjacent BN segment. In Fig. 4.19 (b), the dispersive minibands and non-dispersive quantum well states are clearly seen. That these quantum well states are confined in the graphene zone (which has small band gap as compared to the band gap of BN ribbon) are demonstrated by isosurface plots of charge densities. In contrast to the confined states, the propagating states have charge densities in both graphene and BN zones of the superlattice. This is another class of heterostructure obtained from graphene based ribbons and their functions can even be advanced by implementing the size modulation in addition to the compositional one.

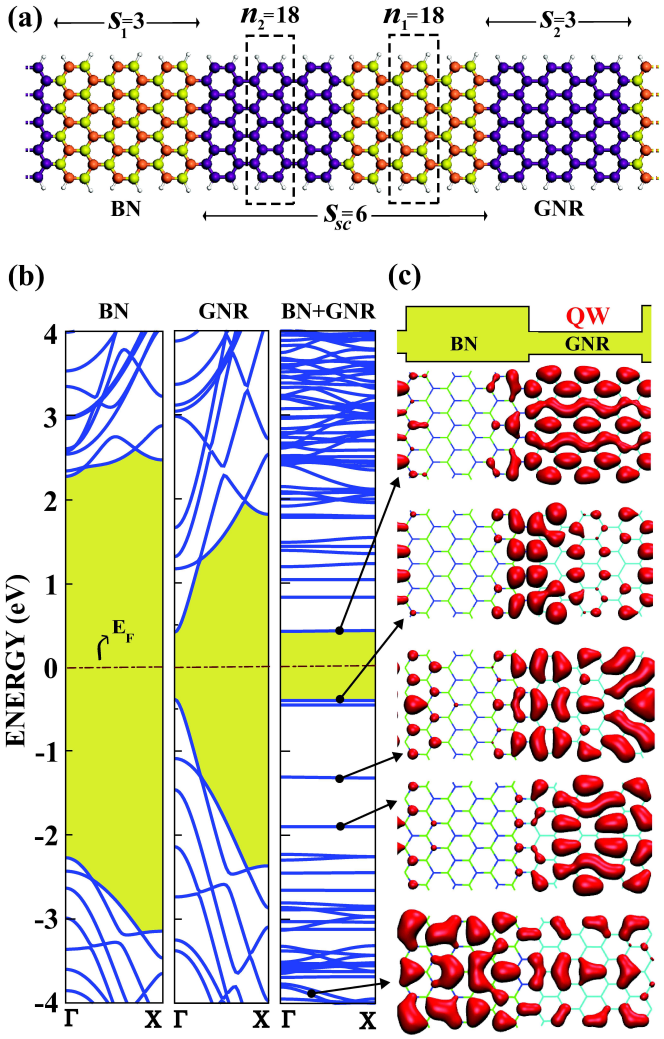

Figure 4.19: One-dimensional superlattice structure formed from the junction of BN and graphene armchair nanoribbons. (a) Atomic structure and superlattice parameters. (b) Band structures of constituent BN and graphene armchair nanoribbons having 18 atoms in their unit cells and the band structure of the superlattice BN(18)/AGNR(18) each segment having 3 unit cells ($s_1 = s_2 = 3$). (c) Energy band diagram in real space forming multiple quantum wells, QW, in graphene segments (zones). Isosurface charge densities of states confined to QW's and propagating states are presented for selected bands.

Chapter 5

Conclusions

Wide range of magnetic and electronic properties of graphene nanoribbons keep the promise of novel nanoscale devices for future applications. The design and fabrication of these devices based on graphene nanoribbons require a proper understanding all the factors that inuence its electronic and magnetic properties. The geometry and vacancy defects are crucial for physical properties of GNRs. The geometry is determined by length, width, edge chirality. Modications of physical properties can be caused by different edge terminations, hetrojunction or defect formations in the ribbon's body. In this thesis, we examined how these factors affect the electronic and magnetic properties of graphene nanoribbons.

A detailed analysis of bare and hydrogenated ribbons with armchair and zigzag edge chirality have been performed. We have verified that the chirality and width of graphene nanoribbons are the two main factors defining the electronic and magnetic properties by our calculations. The inverse proportionality of band gaps with the ribbon width is a characteristic feature for both armchair and zigzag shaped nanoribbons. Our studies reveal that vacancy formation is also a factor influencing the electronic and magnetic properties. An armchair graphene nanoribbon is a nonmagnetic material throughout its structure. But our studies show that a single defect can provide an induced magnetism on it. On the other hand, a zigzag shaped graphene nanoribbon has an antiferromagnetic order and a single defect can break that order leading to a ferrimagnetic ground state.

Two different electronic states are distinguished: These are: (i) itinerant states perturbed by defects, (ii) defect induced states. While the former is dispersive, the latter give rise to flat bands. The reconstruction and spin-polarization of the orbitals at the close proximity of the defect give rise to net magnetic moments, which, in turn, change the magnetic ground state of the defect-free ribbon. Even a semiconductor armchair ribbon can be turned into a metallic ribbon through defect formation. By manipulating the defect formation through irradiation one can tune the electronic and magnetic properties of graphene nanoribbons. Modulation of band gaps of graphene nanoribbons are also possible through defect formation. For example the band gap of an armchair graphene nanoribbon having 34 carbon atom in its unit cell can be changed from 0.1 eV to a 0.4 eV by forming a hexagonal defect in the middle of the ribbon. Our further analysis showed that modulation of band gaps depends on the position of the defect created on the ribbon.

We showed that periodically repeated junctions of segments of graphene nanoribbons with different widths can form stable superlattice structures. This is a one-dimensional analog of two-dimensional, pseudomorphic or commensurate semiconductor superlattices. These new type of heterostructures show a clear evidence of charge confinement in multiple quantum well structures obtained from graphene nanoribbons. Orientation of constituent nanoribbons, their width and length, the symmetry of the junction are some of the structural parameters to engineer electronic properties of these structures. We have performed very detailed analysis of these parameters. Our results revealed that energy band gap and confined states of the superlattices are modulated in real space by varying the geometrical parameters. We also show that in addition to the size modulation, periodically repeating heterostructures of BN/Graphene armchair nanoribbon can also result in multiple quantum well structures with minibands and confined states.

Together with the unique electronic and transport properties of graphene, the quantum-well structures of graphene ribbons offer a basis for investigating problems in nanoscale physics and realizing graphene-based electronics.

Bibliography

[1] F.P. Bundy *et.al* , Carbon, Volume **34**, Number 2, (1996)

[2] L. D. Landau, Zur Theorie der phasenumwandlungen II. Phys. Z. Sowjetunion 11, 2635 (1937)

[3] R. E. Peierls, Ann. I. H. Poincare 5, 177222 (1935)

[4] Landau, L. D. and Lifshitz, E. M. Statistical Physics, Part I (Pergamon, Oxford, 1980)

[5] N. D. Mermin, Phys. Rev. **176**, 250254 (1968)

[6] J. A. Venables *et.al*, Rep. Prog. Phys. **47**, 399459 (1984)

[7] Nelson, D. R., Piran, T. & Weinberg, S. Statistical Mechanics of Membranes and Surfaces (World Scientific, Singapore, 2004)

[8] K. S. Novoselov *et.al*, Science **306**, 666 (2004)

[9] K. S. Novoselov *et.al*, Nature **438**, 197 (2005)

[10] Y. Zhang *et.al* , Nature **438**, 201 (2005)

[11] M. I. Katsnelson *et.al*, Nature Physics **2**, 620 (2006)

[12] X. Li *et.al* , Science **319**, 1229 (2008)

[13] K. S. Novoselov *et.al*, Nature Materials **6**, 183 (2007)

[14] S. Stankovich *et.al*, Nature **442** , 282 (2006)

[15] F. Schedin *et.al*, Nature Materials **6**, 652 (2007)

[16] C. Ataca, E. Akturk and S. Ciraci, High Capacity Hydrogen Storage by Metallized Graphene, submitted to APL.

[17] H. Sevincli *et.al*, Phys. Rev. B **77**, 195434 (2008)

[18] P. R. Wallace, Phys. Rev. **71**, 622 (1947)

[19] Z. H. Ni, *et.al*, Phys. Rev. B **77**, 115416 (2008)

[20] C. Casiraghi *et.al*, Nano Lett. **7**, 2711 (2007)

[21] M. Y. Han *et.al*, Phys. Rev. Lett. **98**, 206805 (2007)

[22] C. Berger *et.al*, Science **312**, 1191 (2006)

[23] C. Berger *et.al*, J. Phys. Chem. B **108**, 19912 (2004)

[24] F. Varchon *et.al*, Phys. Rev. Lett. **99**, 126805 (2007)

[25] A. Mattausch *et.al* , Phys. Rev. Lett. **99**, 076802 (2007)

[26] J. Hass *et.al*, Phys. Rev. B **75**, 214109 (2007)

[27] W. Chen *et.al* , Surf. Sci. **596**, 176 (2005)

[28] P. Hohenberg and W. Kohn, Phys. Rev. **136**, B864 (1964)

[29] W. Kohn and L. J. Sham, Phys. Rev. **140**, A1133 (1965)

[30] L. H. Thomas, Proc. Cambridge. Philos. Soc. **23**, 542 (1927)

[31] E. Fermi, Z. Phys. **48**, 73 (1928)

[32] P.Fulde Electron Correlations in Molecules and Solids Springer-Verlag,Berlin. (1993)

[33] J.Perdew Intl. J. Quant. Chem **57**, 309 (1996)

[34] D. R. Hamann Phys. Rev. Lett. **76** 660 (1996)

[35] J. P. Perdew and Y. Wang, Phys. Rev. B, **45**, 13244 (1991)

[36] C. Kittel *Introduction to Solid State Physics* (Wiley and Sons, New York, 1996)

[37] H.J. Monkhorst and J.D. Pack, Phys. Rev. B **13**, 5188, (1976)

[38] X. Wang *et al.*, Phys. Rev. Lett. **100**, 206803 (2008)

[39] Numerical computations have been carried out by using VASP software:G. Kresse, J. Hafner, Phys Rev. B **47**, 558 (1993); G. Kresse, J. Furthmuller, Phys Rev. B **54**, 11169 (1996)

[40] H.J. Monkhorst and J.D. Pack, Phys. Rev. B **13**, 5188 (1976)

[41] Y-W Son *et al.*, Phys. Rev. Lett. **97**, 216803 (2006)

[42] Y-W Son *et al.*, Nature **444**, 347 (2006)

[43] V. Barone *et al.*, Nano Lett. **6**, 2748 (2006)

[44] M. Fujita *et al.*, J. Phys. Soc. Jpn. **65**, 1920 (1996)

[45] K. Wakabayashi *et al.*, Rev. B **59**, 8271 (1999)

[46] A. Hashimoto *et al.*, NATURE **343**, 870 (2004)

[47] P. O. Lehtinien *et al.*, Phys. Rev. Lett. **93**, 187202 (2004)

[48] P. Esqinazi, *et al.*, Phys. Rev. Lett. **91**, 227201 (2003)

[49] O. V. Yazyev and L. Helm, Phys. Rev. B **75**, 125408 (2007)

[50] E.H. Lieb, Phys. Rev. Lett. **62**, 1201 (1989)

[51] Esaki, L.; Chang, L. L.; Phys. Rev. Lett. **33**, 495 (1974)

[52] Bastard, G.; *"Wave mechanics applied to semiconductor heterostructures"*, Les Editions de Physique, Les Ullis, France, (1988)

[53] Ciraci, S.; I. P. Batra, Phys. Rev. Lett. **58**, 1982 (1987)

[54] Ciraci, S.; Batra, I. P.; Phys. Rev. B **36**, 1225 (1987)

[55] Ciraci, S.; Batra, I. P.; Phys. Rev. B **38**, 1835 (1988)

[56] Ciraci, S.; Baratoff, A.; Batra, I. P.; Phys. Rev. B **41**, 2763 (1990)